

# Dramatic biome changes in China through the Cenozoic Era: Modeling the combined effects of climate, CO<sub>2</sub> concentration, and topography on long-term vegetation dynamics

Jie Xia <sup>a</sup>, Kai Li <sup>a</sup>, Mengna Liao <sup>a</sup>, Zihua Tang <sup>b</sup>, Dongmei Yang <sup>a</sup>, Jian Ni <sup>a,\*</sup>

<sup>a</sup> College of Life Sciences, Zhejiang Normal University, Jinhua, China

<sup>b</sup> Institute of Geology and Geophysics, Chinese Academy of Sciences, Beijing, China

## ARTICLE INFO

Editor: Howard Falcon-Lang

### Keywords:

BIOME4-Asia  
Climate change  
Atmospheric CO<sub>2</sub> concentration  
Topographic evolution  
Cenozoic

## ABSTRACT

Past vegetation patterns and dynamics reflect changes to the environment, climate, and human disturbance over time. As such, they comprise potential analogues for vegetation development under future climate change scenarios. Simulations of global and regional vegetation patterns in the present and future are well established; however, such simulations, especially over geological time-scales, have been remain relatively rare for China. Here, we used proxy-based reconstructions of paleoclimate, atmospheric CO<sub>2</sub> concentration, and topography (including uplift of the Tibetan Plateau (TP)) to drive an improved version of the global vegetation model BIOME4-Asia. Our aim was to simulate paleovegetation changes across China throughout the Cenozoic and to examine the combined effects of these factors on long-term vegetation dynamics. The simulations revealed dramatic shifts in biome distribution and coverage under varying climatic, CO<sub>2</sub>, and elevational conditions. Catastrophic regime shifts occurred in response to sudden, pronounced environmental changes during several intervals. Forest biomes expanded northward and westward, with increased coverage, during warm and humid climates, high pCO<sub>2</sub>, and lower TP elevation, especially between 66 Ma and 40 Ma. Conversely, forests retreated southward, grassland and desert biomes advanced eastward, and dry tundra expanded on the plateau during colder and drier climates, reduced pCO<sub>2</sub>, and higher elevations, particularly between 2 Ma and 21 ka. During other periods, simulated biomes broadly resembled modern distributions. Overall, climate change, atmospheric CO<sub>2</sub> concentration, and TP uplift jointly shaped vegetation dynamics in China during the Cenozoic, consistent with model simulations, pollen and macrofossil evidence, and phylogenomic studies. Incorporating paleoclimate data from advanced climate model simulations, paleotopography and land-sea reconstructions, and paleosol properties will be critical for reducing modeling uncertainties in future work.

## 1. Introduction

Paleovegetation is a key to understanding past environmental changes and their driving mechanisms, including climate change, topographical evolution, and human disturbance. It also provides the foundation for exploring the co-evolution of paleoflora, paleofauna, and paleobiodiversity. Accordingly, the investigation of past vegetation dynamics in relation to climate change has become a central theme in global change research (Nolan et al., 2018; Fordham et al., 2020; Tierney et al., 2020).

Two major approaches have been widely applied to reconstruct geographical patterns of vegetation across historical and geological time

slices. One is based on pollen and macrofossil records, qualitatively or quantitatively, by compiling extensive site-specific data worldwide. This approach enables regional land-cover reconstruction using the Landscape Reconstruction Algorithm (Sugita, 2007a, 2007b) and continental to global biome reconstruction through the Biomization technique (Prentice et al., 1996; Prentice and Webb III, 1998; Prentice and Jolly, 2000). The second approach uses simulations derived from regional or global vegetation models, which are often employed to predict future vegetation dynamics. These models may be biogeographical or biogeochemical, statistical or mechanistic, and have also been applied to paleovegetation, for example, global vegetation patterns in the Middle Pliocene (Salzmann et al., 2008), over the past 140,000 years (Allen

\* Corresponding author at: College of Life Sciences, Zhejiang Normal University, Yingbin Avenue 688, Jinhua 321004, Zhejiang Province, China.  
E-mail address: [nijian@zjnu.edu.cn](mailto:nijian@zjnu.edu.cn) (J. Ni).

et al., 2020), and from the Middle to Late Pleistocene (Huntley et al., 2023).

Vegetation models, whether steady or dynamic, empirical or process-based, have become indispensable tools for examining past, present, and future terrestrial ecosystem dynamics. They provide insight into biochemical and biophysical interactions between ecosystems and the atmosphere, particularly carbon cycles, and they form integral components of Earth system models. Among them, the BIOME family of terrestrial ecosystem models is one of the most widely used. BIOME1 was purely biogeographical (Prentice et al., 1992), whereas BIOME2 introduced biogeochemical processes (Haxeltine et al., 1996). BIOME3 (Haxeltine and Prentice, 1996) and BIOME4 (Kaplan, 2001; Kaplan et al., 2003) coupled biogeographical and biogeochemical mechanisms, and LPJ (Sitch et al., 2003) extended the framework into a dynamic global vegetation model. These models have not only shaped global vegetation prediction for the past, present, and future, but have also been successfully applied to regional simulations, including vegetation in China under present and future scenarios (Ni, 2000; Ni et al., 2000; Ni and Herzschuh, 2011; Zhao and Wu, 2014; Gao et al., 2016) and in Asia under past conditions (Dallmeyer et al., 2017).

The Cenozoic Era, spanning from 66 Ma to the present, represents the third major era of Earth's history. It is characterized by the modern arrangement of continents (Prothero, 2021), rapid changes in atmospheric CO<sub>2</sub> concentrations and climate (Tierney et al., 2020; Westerhold et al., 2020), and the accelerated evolution of mammals, birds, and angiosperms toward modern forms (Stiller et al., 2024; Zuntini et al., 2024). Early Cenozoic climates were considerably warmer than today, with peak warmth during the Paleocene–Eocene Thermal Maximum (PETM). In contrast, the Eocene–Oligocene Transition (EOT) and Quaternary glaciations were cooler and drier (Tierney et al., 2020; Westerhold et al., 2020). The explosive radiation of angiosperms during the Cenozoic was a defining event that drove the establishment of modern vegetation patterns: deciduous species dominated in cold regions, whereas evergreen species thrived in the subtropics and tropics (Prothero, 2021). Understanding vegetation shifts across the Cenozoic is therefore essential for tracing the origins of modern biodiversity. However, most studies have focused on fossil-rich sites or on short time intervals in the late Cenozoic (e.g., Salzmann et al., 2008; Allen et al., 2020; Huntley et al., 2023). The absence of continuous vegetation simulations covering the full Cenozoic limits deeper insights into the interplay among geology, climate, and vegetation at geological time scales.

In East Asia, particularly in China, rapid changes in atmospheric CO<sub>2</sub>, climate, and biodiversity were closely linked to dramatic geological events. The uplift of the Tibetan Plateau (TP) (Li and Fang, 1999; Tapponnier et al., 2001; Royden et al., 2008; Wang et al., 2008; Su et al., 2019) profoundly altered the East Asian monsoon system (Farnsworth et al., 2019a; Wang et al., 2020), reshaped biodiversity (Ding et al., 2020; Spicer et al., 2020), and influenced the expansion of steppe–desert vegetation (Barbolini et al., 2020). China's vast area and pronounced horizontal and vertical bioclimatic gradients make it an ideal testing ground for vegetation models. While potential vegetation distributions and future scenarios have been widely simulated, reconstructions of past vegetation have mainly focused on the last 20 ka BP (e.g., Ni et al., 2014; Li et al., 2019; Cao et al., 2022). High-quality continuous pollen and macrofossil records extending into deep time remain scarce (Wang et al., 2012; Fan et al., 2020; Zhao et al., 2020), and continuous vegetation dynamics over long geological periods have rarely been reported.

Two central questions remain: how did past changes in climate and atmospheric CO<sub>2</sub> affect vegetation patterns and biome shifts, and how did the uplift of the TP modulate climate and vegetation responses? To address these questions, we simulated vegetation patterns in China throughout the Cenozoic using the improved global vegetation model BIOME4-Asia. Our simulations account for climate, atmospheric CO<sub>2</sub>, and topographical changes. The aim was not to reconstruct the “real” vegetation distribution for specific geological stages, as the driving

environmental data were artificially generated, but rather to examine the combined effects of long-term changes in climate, atmospheric CO<sub>2</sub>, and topography on vegetation dynamics, and to provide a baseline for exploring interactions among deep-time climate change, vegetation shifts, and biodiversity evolution.

## 2. Methods

### 2.1. Regional improvement of the global vegetation model BIOME4

We used BIOME4, a steady-state vegetation model from the BIOME family, rather than the dynamic vegetation model LPJ, to simulate past vegetation in China. This choice was made because our focus was on vegetation at discrete time slices rather than continuous time series. BIOME4 (Kaplan, 2001; Kaplan et al., 2003) is an equilibrium global vegetation model that integrates biogeographical and biogeochemical processes to predict vegetation distribution, structure, and functions, including carbon and water fluxes. The model incorporates 13 plant functional types (PFTs) and simulates soil water balance, canopy conductance, photosynthesis, respiration, and phenology to determine the seasonal maximum leaf area index (LAI) that maximizes net primary productivity (NPP) for each PFT. Using these calculations, BIOME4 predicts 28 global biomes (Kaplan, 2001). The model is driven by monthly mean temperature, precipitation, sunshine percentage (cloudiness), and absolute minimum temperature. It is sensitive to changes in climate and atmospheric CO<sub>2</sub> concentration due to the responses of NPP and stomatal conductance to CO<sub>2</sub> and the differential effects of CO<sub>2</sub> enrichment on C<sub>3</sub> and C<sub>4</sub> plants (Kaplan, 2001).

In the original BIOME4 model, five tundra biomes were refined to improve simulations of Arctic vegetation (Kaplan et al., 2003). A subsequent variant, BIOME4-Tibet, was designed to better represent alpine vegetation on the TP by modifying key bioclimatic and ecophysiological parameters (Ni and Herzschuh, 2011). BIOME4-Asia introduced further improvements, particularly in the rules distinguishing steppe and desert biomes in Central Asia, and incorporated the influence of topography (elevation) on vegetation distribution in high mountains and plateaus (Dallmeyer et al., 2017). The effectiveness of BIOME4 in simulating China's vegetation has been verified (Wang et al., 2011), supporting its use in both global and regional biome simulations. In this study, we applied the BIOME4-Asia version (Dallmeyer et al., 2017) to simulate past vegetation in China. Because the performance of this model has been demonstrated in earlier work, we did not re-compare modeled potential vegetation with observed vegetation maps. For analysis, the 28 simulated biomes were consolidated into nine mega-biomes (Table 1), following the approach of Harrison and Prentice (2003) and Wang et al. (2011).

### 2.2. Time slices

We established 37 key time slices, including the present, to simulate changes in biome distribution across China (Table 2). The temporal resolution was 1 ka during the Holocene, 1 Ma from the Pleistocene to the Pliocene, 5 Ma during the Miocene, and 10 Ma during the Paleogene. Additional key intervals corresponding to major geological and biological events were also selected.

### 2.3. Input data

#### 2.3.1. Climates

Vegetation prediction is generally driven by observed historical climate data, and paleovegetation distribution should ideally be simulated using paleoclimate data, such as those generated by general circulation models (GCMs). However, continuous deep-time paleoclimate simulations are still scarce. The longest continuous simulation we identified was 0.12 Ma using HadCM3 (Beyer et al., 2020), later extended statistically to 0.8 Ma (Krapp et al., 2021). Another HadCM3

**Table 1**

Biomes simulated by the BIOME4-Asia model and their assignment into megabiomes.

Biome	Mega-biome
Tropical evergreen forest	Tropical forests
Tropical semi-deciduous forest	Tropical forests
Tropical deciduous forest/woodland	Tropical forests
Warm mixed forest	Warm-temperate forests
Temperate deciduous forest	Warm-temperate forests
Temperate conifer forest	Temperate forests
Cool mixed forest	Temperate forests
Cool conifer forest	Temperate forests
Cold mixed forest	Temperate forests
Evergreen taiga/montane forest	Boreal forests
Deciduous taiga/montane forest	Boreal forests
Boreal parkland	Boreal forests
Tropical savanna	Savanna and dry woodland
Temperate broadleaved savanna	Savanna and dry woodland
Temperate sclerophyll woodland	Savanna and dry woodland
Open conifer woodland	Savanna and dry woodland
Tropical xerophytic shrubland	Grassland and dry shrubland
Temperate xerophytic shrubland	Grassland and dry shrubland
Tropical grassland	Grassland and dry shrubland
Temperate grassland	Grassland and dry shrubland
Desert	Desert
Barren	Desert
Steppe tundra	Dry tundra
Shrub tundra	Dry tundra
Dwarf shrub tundra	Dry tundra
Prostrate shrub tundra	Wet tundra
Cushion forb, lichen and moss tundra	Wet tundra
Land ice	

study extended simulations back to 150 Ma, but only at selected key time slices, with parts of the results derived from modeling experiments (Farnsworth et al., 2019a, 2019b). Other long-term climate studies, such as those for 66 Ma (Westerhold et al., 2020) and 100 Ma (Tierney et al., 2020), were reconstructed primarily from proxy data. These reconstructions mainly provided mean annual temperature, without resolving regional or global geographical patterns. By contrast, more recent past climates have been better represented in transient simulations. Examples include the TRACE21 model and the CHELSA-TraCE21k dataset for the last 21 ka (Karger et al., 2023), and the EC-Earth3-LR simulations of warm periods at selected time slices such as the mid-Pliocene (3 Ma), the last interglacial (129–116 ka), and the mid-Holocene (6 ka) (Zhang et al., 2021). However, these efforts remain either too short in temporal coverage or too limited in time slices to satisfy the requirements of our study. Furthermore, most of the above simulations provided only temperature and precipitation, but lacked variables such as sunshine percentage (cloudiness) and absolute minimum temperature, which are essential inputs for our model.

Because paleoclimate simulations were insufficient or inconsistent across the full Cenozoic, using them directly to drive vegetation modeling would have required combining inputs from multiple sources. Such an approach would not have been reasonable within a single modeling framework. Given this limitation and the primary objective of our study, we adopted a quasi-paleoclimate approach. We used modern observed climate records (averaged for 1980–2010) from 2152 meteorological stations across China (China Meteorological Data Service Centre, <http://data.cma.cn>). Four variables (monthly temperature, precipitation, sunshine percentage, and absolute minimum temperature) were interpolated into 10 km grid cells using a thin-plate smoothing spline technique (Hancock and Hutchinson, 2006; Xu and Hutchinson, 2013) in ANUSPLIN 4.4 (Hutchinson and Xu, 2013). This method accounts for the influence of elevation, using the Shuttle Radar Topography Mission (SRTM) digital elevation model (DEM; Farr et al., 2007). Past climate differences for each geological time slice (Table 2) were superimposed onto modern climate data to generate climate forcing for vegetation simulations. Deep-time temperature anomalies

(pre-Pleistocene) were derived from global reconstructions at 66 Ma (Westerhold et al., 2020) and 100 Ma (Tierney et al., 2020), while Holocene anomalies were obtained from regional integrations (Zhu, 1973; Shi and Kong, 1992). Numerical reconstructions of past precipitation are much rarer. For East Asia, precipitation changes were estimated using simulations (Farnsworth et al., 2019a) and reconstructions (Wang et al., 2020), supplemented by the empirical relationship between precipitation and temperature (a 7 % increase in precipitation per 1 K warming; Held and Soden, 2006) when paleoprecipitation information was unavailable. Past cloudiness was assumed to remain constant at modern levels, due to the absence of data and the relatively minor role of this variable in determining vegetation distribution in the model.

Seasonal variations of past temperature and precipitation (Table 3) were also incorporated, based on the National Assessment Report on Climate Change (The Editorial Committee of the China's National Assessment Report on Climate Change, 2007) and the Blue Book on Climate Change in China 2020 (The Climate Change Center of China Meteorological Administration, 2020). These seasonal adjustments were applied to each time slice. The magnitude of warming differs by season, with stronger warming in winter compared with spring (IPCC, 2021).

### 2.3.2. Atmospheric CO<sub>2</sub> concentrations

Reconstructed atmospheric CO<sub>2</sub> concentrations were obtained from multi-proxy records (Foster et al., 2017; Tierney et al., 2020; Westerhold et al., 2020) and ice-core data (Lüthi et al., 2008) (Table 2).

### 2.3.3. Soils

The BIOME4 model calculates the water balance of terrestrial ecosystems using soil texture-related water-holding capacity and percolation rate for two layers: the topsoil (0–30 cm) and the subsoil (30–150 cm). Observed water-holding capacity was derived from a 1:1 million soil database of China (Shi et al., 2004), while percolation rates were taken from a global digital soil map used in the original BIOME4 model (Kaplan, 2001), as no regional resource is available. These properties were held constant for all time slices because no reconstructions of past soil parameters exist.

### 2.3.4. Topography and land-sea mask

Paleogeography strongly influences regional and global climate systems (Lunt et al., 2016; Farnsworth et al., 2019a). In East Asia, the uplift of the TP has been a major driver of regional climate and biome dynamics. Although the timing, magnitude, and spatial heterogeneity of TP uplift remain debated, broad consensus exists regarding major elevation changes (Li and Fang, 1999; Tapponnier et al., 2001; Royden et al., 2008; Wang et al., 2008; Su et al., 2019; Spicer et al., 2020). Changes in the land-sea mask also shaped climate and vegetation, particularly in coastal and low-lying areas. During the early and middle Cenozoic, continental drift and climate change produced land-sea configurations different from those of today (Scotese, 2021). The PALEOMAP PaleoAtlas (Scotese, 2016, 2021) provides paleogeographical reconstructions of topography and bathymetry for 93 geological stages since the Middle Neoproterozoic (750 Ma), including 17 maps spanning the present to the K/Pg boundary (66 Ma). These maps are widely regarded as the most comprehensive global paleogeographical resource.

Despite their utility, the PaleoAtlas maps could not be directly applied in this study. First, the 17 available maps did not align with our 37 target time slices. Second, vegetation patterns produced under dynamic paleogeography could not be directly compared across slices. Third, because our vegetation model is driven by climate data that already accounts for topography, adding paleogeographical adjustments would have introduced inconsistencies. For these reasons, we did not use PALEOMAP maps. Instead, elevations for each time slice were judged using the present SRTM digital elevation model (Farr et al., 2007) in combination with published consensus on TP uplift. Three regional uplift zones were distinguished: southern TP (latitude <28°N), central TP (28–34°N), and northern TP (34–40°N) (Table 2). The land-sea mask

**Table 2**

Key geological time slices and their setups for the model simulations.

Epoch	Key time slices	Geological time (ka/Ma)	Temperature difference (°C)	Precipitation difference (%)	CO <sub>2</sub> concentration (ppmv)	Elevation change (southern TP)	Elevation change (central TP)	Elevation change (northern TP)
Holocene	Mid-Holocene Climate Optimum (MHCO)	0 ka	0	0	360	0	0	0
		1 ka	-1	-7	280	0	0	0
		2 ka	1	7	280	0	0	0
		3 ka	0.5	3.5	280	0	0	0
		4 ka	1.2	8.4	270	0	0	0
		5 ka	1.5	10.5	270	0	0	0
		6 ka	3	21	270	0	0	0
		7 ka	2	14	260	0	0	0
		8 ka	0.8	5.6	260	0	0	0
		9 ka	-0.5	-3.5	260	0	0	0
		10 ka	-1.2	-8.4	260	0	0	0
Pleistocene	Last Glacial Maximum (LGM)	21 ka	-4	-28	190	0	0	0
		1 Ma	-3	-21	260	-500	-500	-300
		2 Ma	-2	-14	290	-1000	-800	-500
		3 Ma	0.6	4.2	320	-2000	-1000	-600
		3.3 Ma	2	14	400	-2000	-1000	-600
Pliocene	Mid-Pliocene Warm Period (MPWP)	4 Ma	0.5	3.5	350	-2500	-1500	-800
		4.4 Ma	3	21	340	-2500	-1500	-800
		5 Ma	0.8	5.6	350	-3000	-2000	-1000
		7 Ma	0.7	4.9	340	-3500	-2500	-1200
		10 Ma	1.5	10.5	345	-3500	-2500	-1200
Miocene	Mid-Miocene Climate Optimum (MMCO)	15 Ma	4	28	390	-3500	-2500	-1200
		17 Ma	5	35	425	-3750	-2750	-1350
		20 Ma	4	28	410	-3750	-2750	-1350
		23 Ma	4	28	430	-3750	-2750	-1350
Oligocene	Oligocene-Miocene Transition (OMT)	24 Ma	4.5	31.5	440	-3750	-2750	-1350
		25 Ma	4	28	580	-4000	-3000	-1500
		28 Ma	4	28	710	-4000	-3000	-1500
		35 Ma	6	42	765	-4000	-3000	-1500
Eocene	Middle Eocene Climate Optimum (MECO)	36 Ma	5	35	1100	-4250	-3500	-1850
		40 Ma	12	84	800	-4250	-3500	-1850
		45 Ma	10	70	780	-4250	-3500	-1850
		50 Ma	14	98	1100	-4500	-4000	-2200
		55 Ma	12	84	740	-4500	-4000	-2200
Paleocene	Paleocene-Eocene Thermal Maximum (PETM)	56 Ma	22	154	1000	-4500	-4000	-2200
		65 Ma	11	77	475	-4500	-4000	-2200
		66 Ma	13	91	800	-4500	-4000	-2200

**Table 3**

Setup of seasonal variations of past changes of temperature and precipitation.

Climate changes	Winter (December–February)	Spring (March–May)	Summer (June–August)	Autumn (September–November)
Mean annual temperature + 1 °C	1.6	1.4	0.3	0.7
Mean annual temperature - 1 °C	-1.6	-1.4	-0.3	-0.7
Mean annual precipitation +1 mm	-0.5	2.5	0.5	-1.5
Mean annual precipitation - 1 mm	0.5	-2.5	-0.5	1.5

was assumed to remain unchanged from present-day conditions.

#### 2.4. Data analysis

Biome maps were produced using GIS software (Fig. 1). Coverage changes of each biome in response to climate variables (temperature and precipitation) were analyzed statistically and visualized in line charts (Fig. 2). The geographical centroid of each biome was calculated by averaging the latitude and longitude of its distribution (Fig. 3).

### 3. Results

During the Holocene, biome distributions in China exhibited patterns broadly similar to the present (Fig. 1a–k). However, savanna and dry woodland, grassland and dry shrubland, and desert biomes expanded eastward into the temperate forest region, reaching maximum coverage (Fig. 2a). The largest eastward shift was approximately 1.5–2° in longitude (Fig. 3a) at 6–7 ka during the mid-Holocene Climatic Optimum (MHCO) (Fig. 2a; Fig. 3e–g), reflecting drier conditions in central and northern eastern China. In contrast, temperate forest coverage

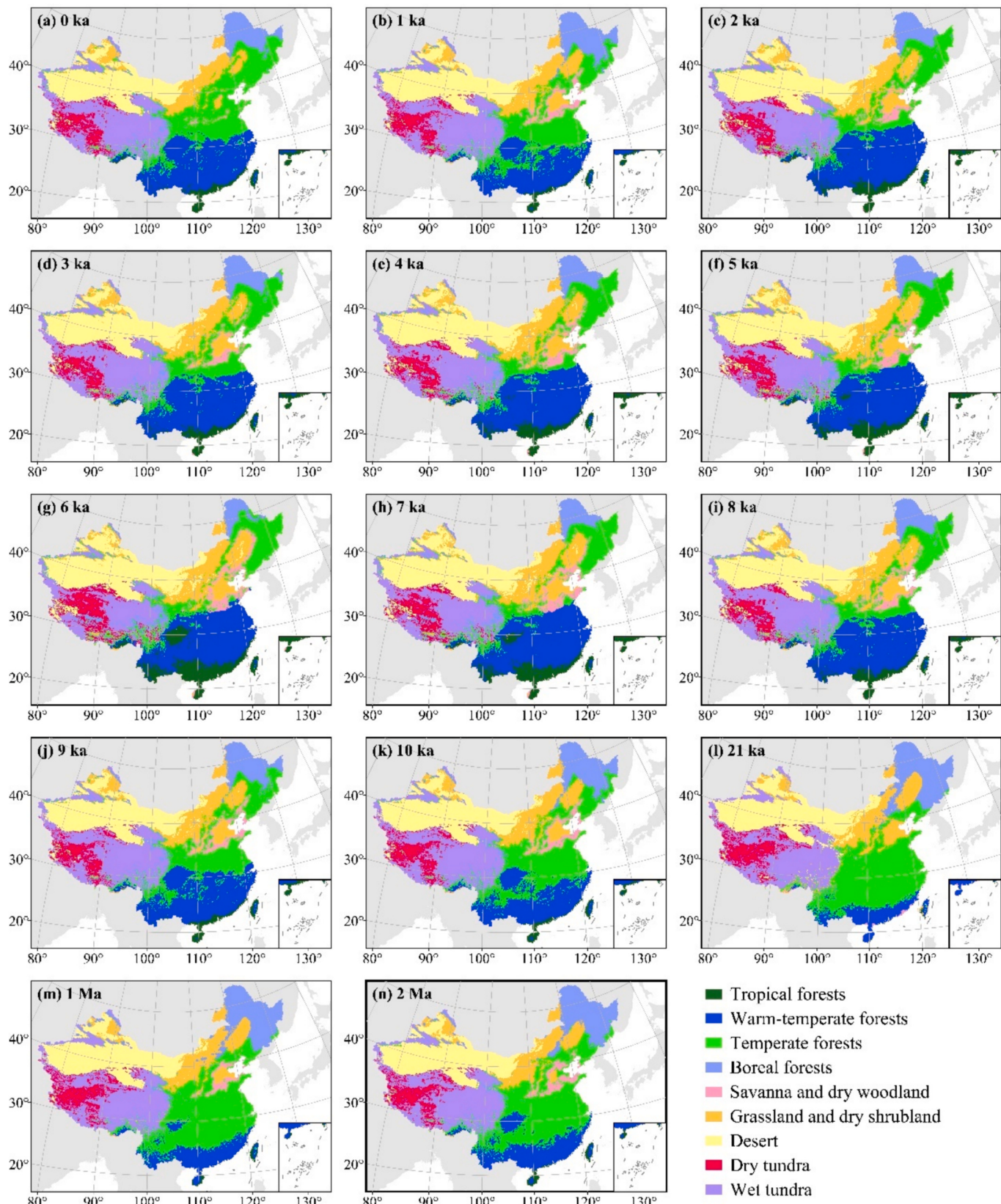


**Fig. 1.** Spatiotemporal distribution of simulated biomes in China during the Cenozoic.

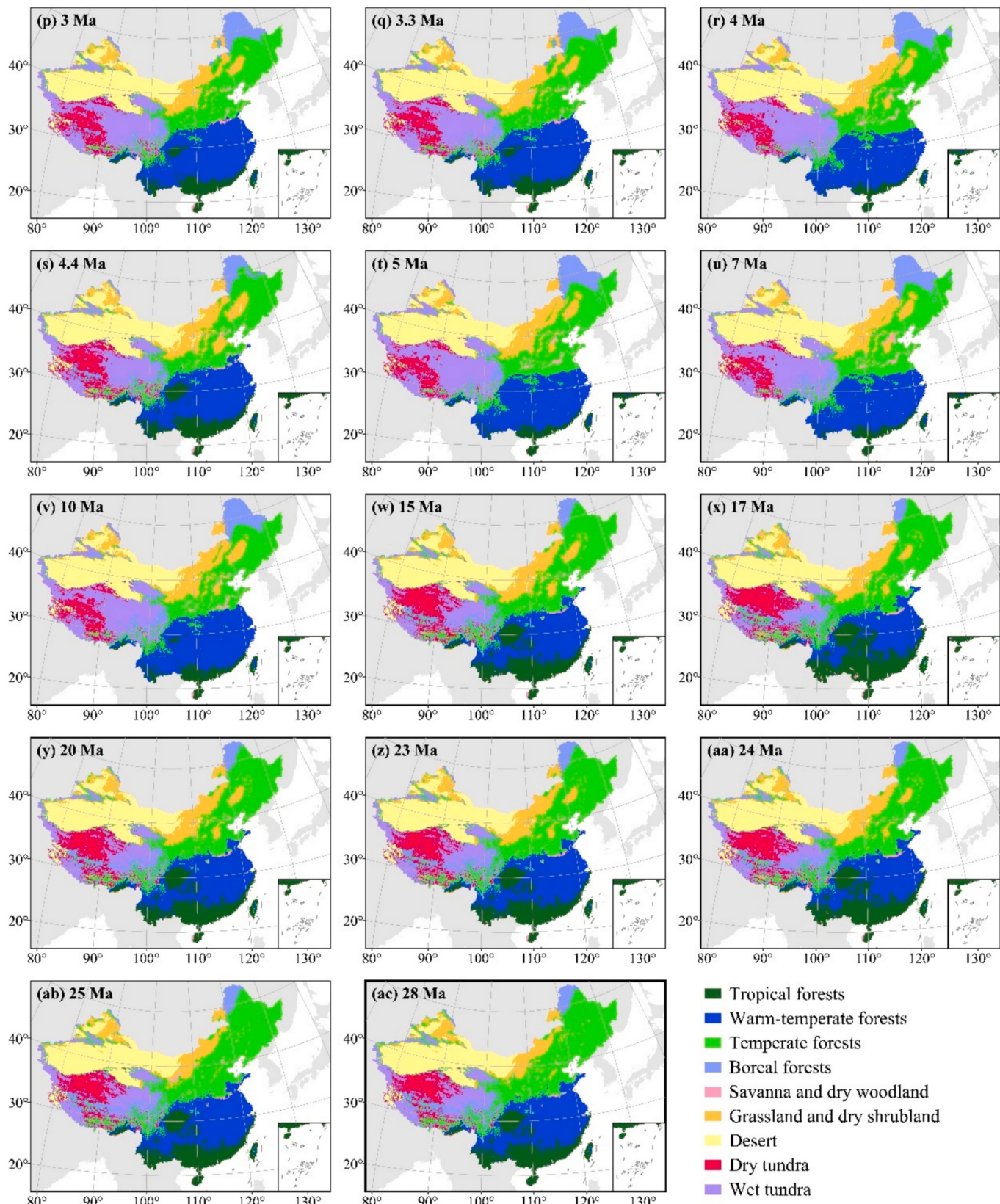


Fig. 1. (continued).

decreased by an average of 6.22 % (Fig. 2c). Between 2 ka and 8 ka, warm-temperate (termed “subtropical” in China) and tropical forest biomes expanded northward, peaking in both coverage and northward

displacement at 5–7 ka during the MHCO (Fig. 2a; Fig. 3a–b). At the same time, temperate forest biomes contracted in central eastern China, while boreal forests declined in northeastern China, with minima in

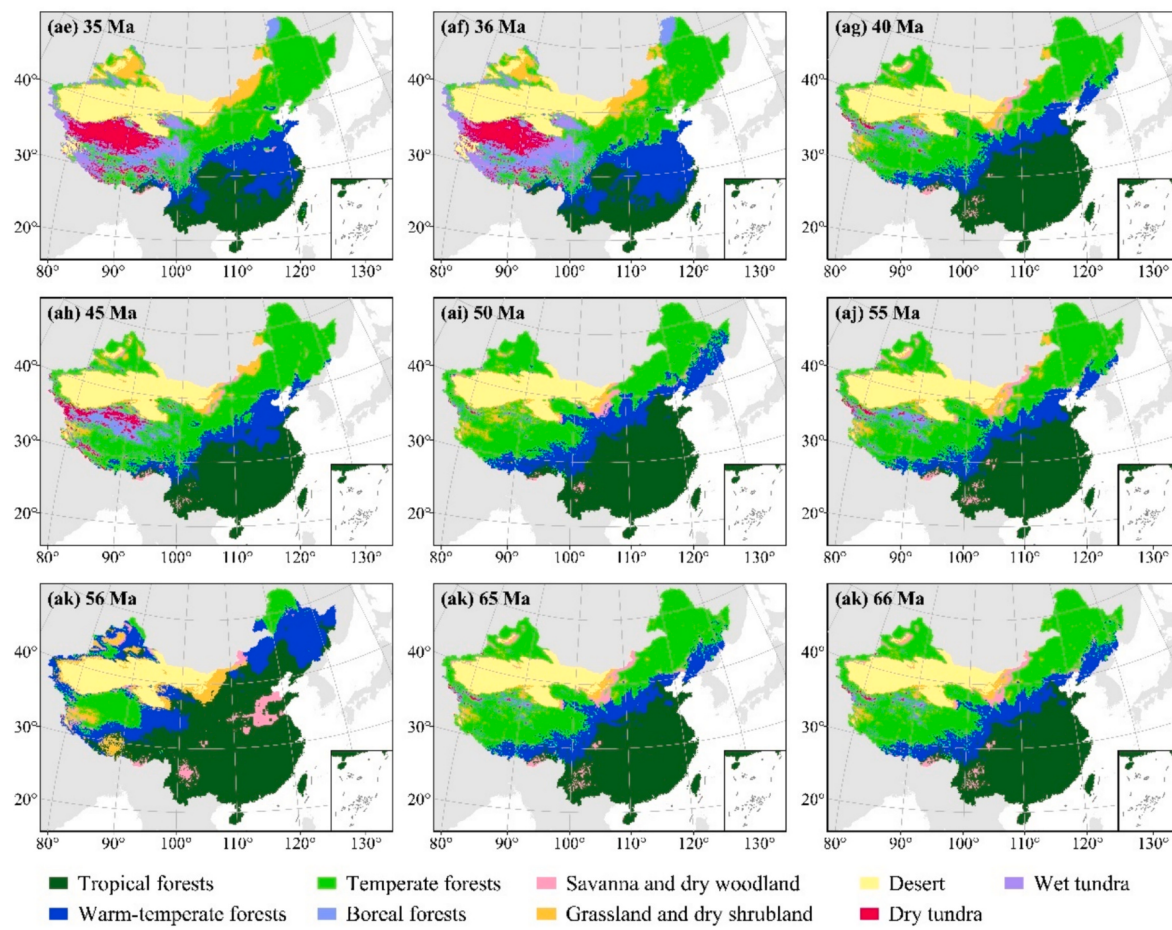


Fig. 1. (continued).

coverage at 6–7 ka (Fig. 2a). These patterns indicate that central and southern eastern China experienced warmer and wetter conditions than at present. Cooler intervals at 1 ka, 9 ka, and 10 ka were marked by southward shifts of forest biomes and reduced coverage of subtropical and tropical forests. The encroachment of temperate forests into subtropical regions also points to drier conditions. On the TP, dry tundra and forest biomes expanded into the wet tundra region, with maximum extent at 6 ka during the MHCO, whereas opposite movements occurred during cooler periods (Fig. 2a; Fig. 3a–d).

Pleistocene biomes (Fig. 1l–n) contrasted sharply with Holocene patterns. During the Last Glacial Maximum (LGM, Fig. 1l), colder temperatures, reduced precipitation, and lower CO<sub>2</sub> levels resulted in a minimum forest coverage of 42.57 % (Fig. 2c). Boreal forests expanded southeastward, while temperate forests advanced southward, with their centroid reaching its southernmost Cenozoic position at ca. 31° latitude (Fig. 3c). Warm-temperate forests retreated sharply, compressing tropical forests, which nearly vanished from mainland China. At this time, warm-temperate forests recorded their lowest coverage (5.14 %; Fig. 2a), with the southernmost centroid at 23.22° latitude (Fig. 3b). Savanna and dry woodland biomes disappeared from central eastern China, surviving only in scattered patches in the south, with a minimum coverage of 0.25 % (Fig. 2a). On the TP, wet tundra expanded eastward and southward at the expense of forests, reaching maximum coverage (18.39 %; Fig. 2a), while dry tundra expanded westward and northward. Biomes at 1 Ma and 2 Ma (Fig. 1m–n) resembled those of the LGM, although tropical forests reappeared on Hainan and Taiwan islands and along southern coastal China. Warm-temperate forests reoccupied the Sichuan Basin, particularly at 2 Ma, and savanna and dry woodland returned to central eastern China.

Pliocene and Miocene biome patterns (Fig. 1o–y) broadly resembled present distributions. Forests dominated eastern China, but during the Mid-Pliocene Warm Period (MPWP, 3.3 Ma), the Pliocene Climatic Optimum (PCO, 4.4 Ma), the mid-Miocene Climatic Optimum (MMCO, 15–17 Ma), and the Early Miocene (20–23 Ma), warmer and wetter conditions combined with elevated CO<sub>2</sub> to drive significant northward expansion of forests, particularly tropical forests. Tropical forests dominated the Sichuan Basin between 3.3 and 4.4 Ma and 15–23 Ma. On the TP, forests advanced northward, occupying much of the eastern and southern plateau. From 15 Ma onward, boreal forests were more extensive on the TP than in northeastern China, though their overall coverage remained constant (Fig. 2a–b). Meanwhile, dry tundra expanded northward and eastward, peaking at 6.84 % at 17 Ma (MMCO; Fig. 2a), while wet tundra contracted. Grassland and desert biomes frequently shifted westward during this period.

During the Oligocene (24–28 Ma), biome distributions were similar to the early Miocene (Fig. 1z–ab). In contrast, the Eocene witnessed major biome reorganization (Fig. 1 ac–ah), driven by climatic fluctuations, TP uplift, and high CO<sub>2</sub>. At the Eocene-Oligocene Transition (EOT, 35–36 Ma; Fig. 1 ac–ad), forests expanded northward. Tropical, warm-temperate, and temperate forests occupied most of eastern China, restricting boreal forests to the northernmost corner of northeastern China. On the TP, however, boreal forests expanded northward, reaching a maximum coverage of 7.47 % at 36 Ma (Fig. 2b). Grassland and dry shrubland contracted sharply along the northern border, while savanna and dry woodland nearly vanished. Desert area also decreased (Fig. 2a). From 40 to 55 Ma (Fig. 1ae–ah), forest biomes advanced northwestward, replacing non-forest types and reaching peak coverage of 82.07 % at 50 Ma (Fig. 2c). Tropical forests expanded northward, dominating warm-

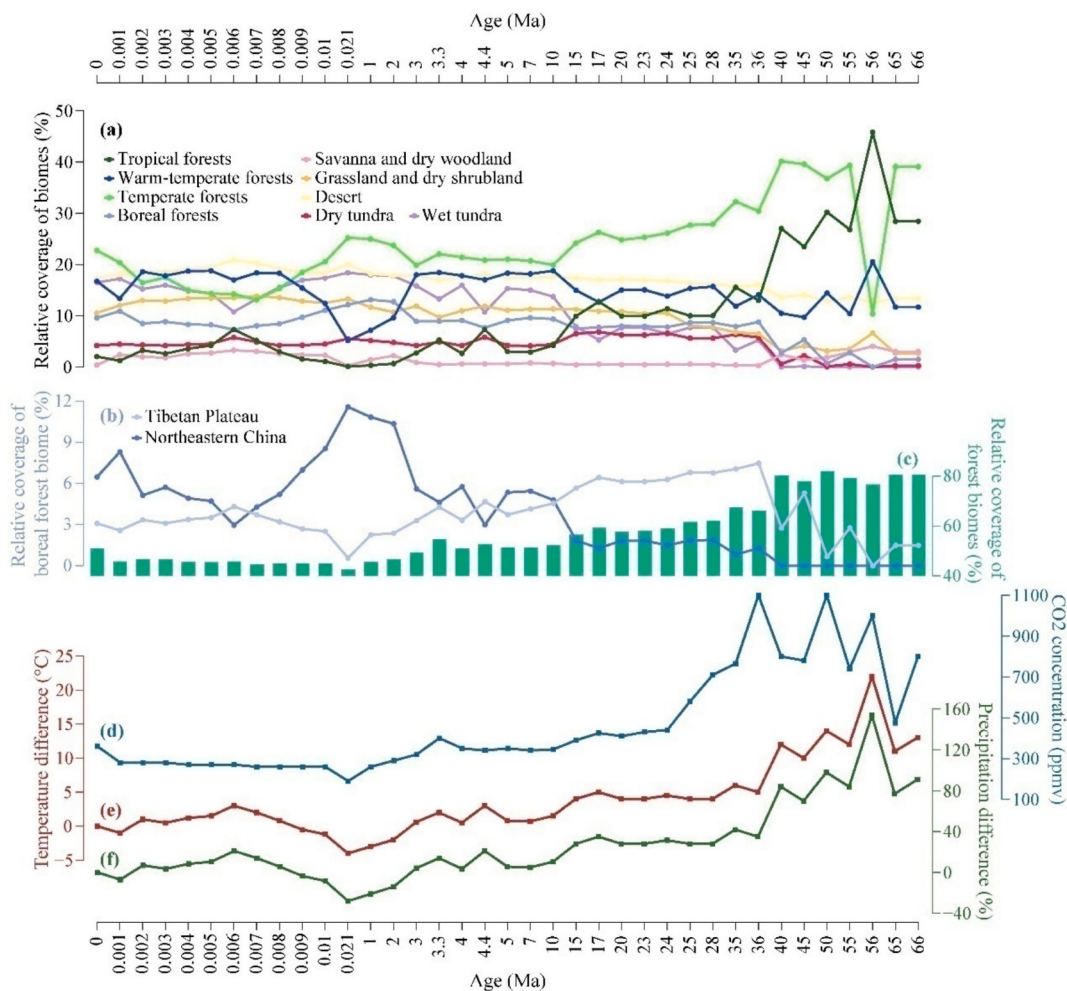


**Fig. 2.** Biome changes in China and their drivers during the Cenozoic. (a) Relative coverage of biomes; (b) Relative coverage of boreal forest on the Tibetan Plateau and in northeastern China; (c) Relative coverage of all forest biomes; (d) Atmospheric CO<sub>2</sub> concentration; (e) Temperature anomalies; (f) Precipitation anomalies.

temperate regions, while warm-temperate forests occupied southern and eastern TP. Temperate forests spread across moist areas of TP and northwestern China, reaching maximum coverage of 40.11 % at 40 Ma (Fig. 2a). Conversely, boreal forests disappeared from northeastern China and declined on TP (Fig. 2b). Grassland, savanna, and shrubland were restricted to narrow bands between forests and deserts or along the southwest border, while deserts north of the Tianshan Mountains and tundra on TP nearly vanished, especially at 50 Ma.

The Paleocene (56 Ma) marked the most dramatic biome shift of the Cenozoic (Fig. 1ai). Tropical forests covered nearly half of China, while warm-temperate and temperate forests, deserts, and small patches of grassland and savanna occupied the remainder. Savanna and dry woodland also appeared within tropical zones. Neither boreal forests nor tundra occurred. Early Paleocene biomes (65–66 Ma) were similar to those at 40 Ma (Fig. 1aj–ak).

#### 4. Discussion

This study applied the BIOME4-Asia global vegetation model to simulate regional vegetation changes across China during the Cenozoic. The model has been improved and validated for accurate biome prediction in China. Because past climate and topographical inputs were “artificial” and past land-sea masks were not incorporated, the simulations should not be interpreted as reconstructions of the “actual” biome distribution at key geological times. Instead, the results highlight the combined effects of climate, atmospheric CO<sub>2</sub>, and topography on long-

term vegetation dynamics. These simulations provide insights into the interactions among climate change, atmospheric composition, and mountain uplift in shaping vegetation patterns.

##### 4.1. Paleobiome changes

Our simulations, based on hypothetical climate change scenarios rather than transient climate model outputs, successfully captured major shifts in the distribution and coverage of forest and non-forest biomes in China (Figs. 1–3). Warm and humid climates, high CO<sub>2</sub> concentrations, and low TP elevation favored northward and westward expansion of forests. By contrast, cold and dry climates, low CO<sub>2</sub> concentrations, and high TP elevation, particularly between 2 Ma and 21 ka, led to southward contraction of forests, eastward shifts of grassland and desert, and eastward expansion of dry tundra on the TP. During intervals of moderate climate, CO<sub>2</sub>, and elevation, biomes showed relatively little departure from modern patterns (Salzmann et al., 2008; Allen et al., 2020).

Comparisons with earlier simulations highlight both consistencies and differences. Salzmann et al. (2008) used BIOME4, driven by HadAM3 climate outputs, to simulate Middle Pliocene (ca. 3 Ma) biomes. Both model and paleobotanical evidence indicated major northward expansion of warm-temperate evergreen and temperate deciduous forests, and penetration of forests into the TP interior, consistent with our findings. However, their study reported a pronounced eastward expansion of temperate grassland, which was not reproduced here. Allen et al. (2020) applied the LPJ-GUESS dynamic global vegetation model,

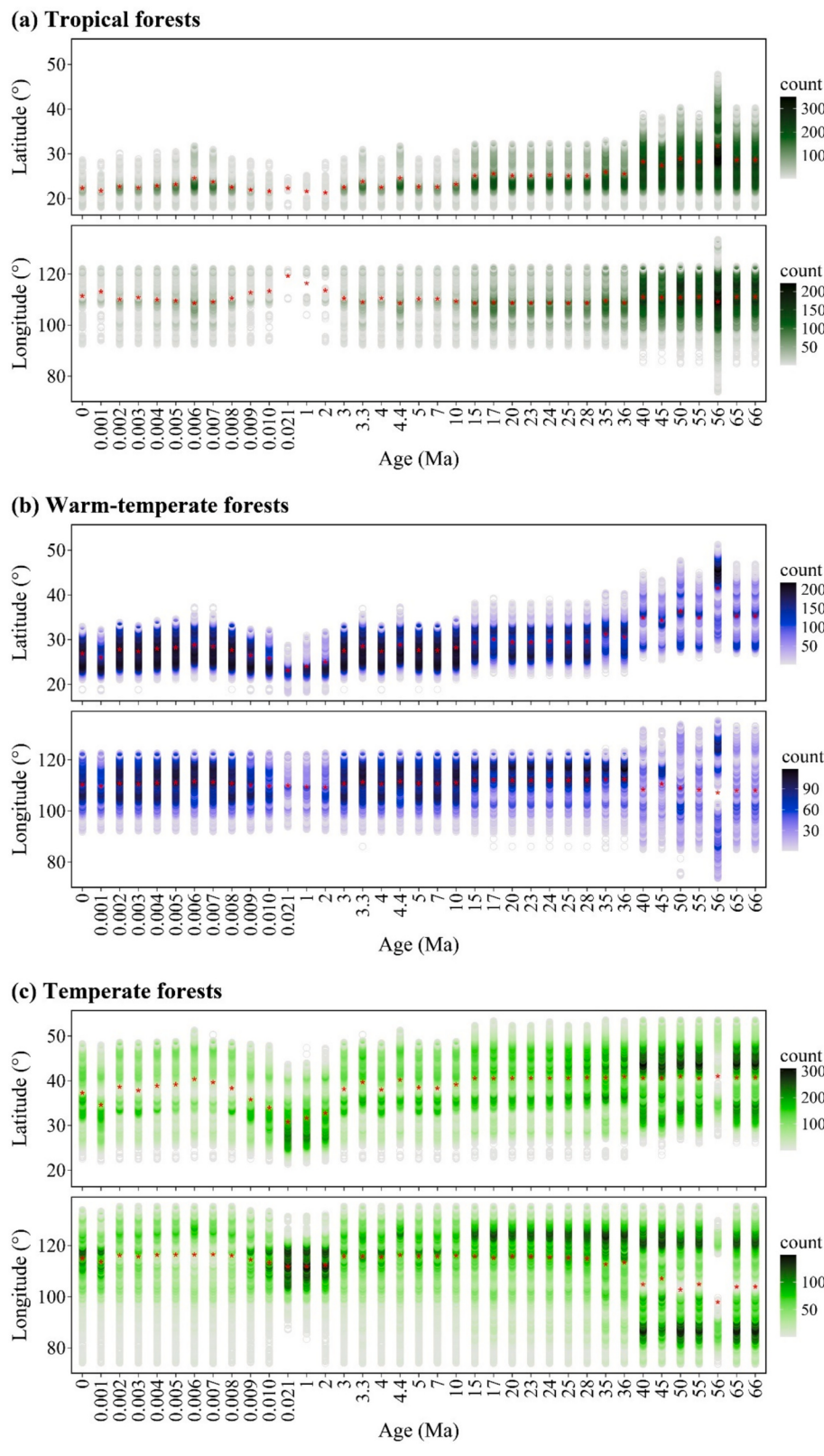


**Fig. 3.** Temporal patterns of latitudinal and longitudinal distribution of simulated biomes in China during the Cenozoic.

driven by ice-core CO<sub>2</sub>, orbital forcing, and HadCM3 paleoclimate, and reported the greatest biome changes in Eurasia, varying on orbital timescales. Their biome patterns at 21 ka and in the Holocene broadly aligned with ours, although coverage differed, likely reflecting

structural differences between BIOME4 and LPJ-GUESS, which share common BIOME family principles.

Pollen evidence from long cores further supports the plausibility of our results. [Barbolini et al. \(2020\)](#) reconstructed steppe–desert

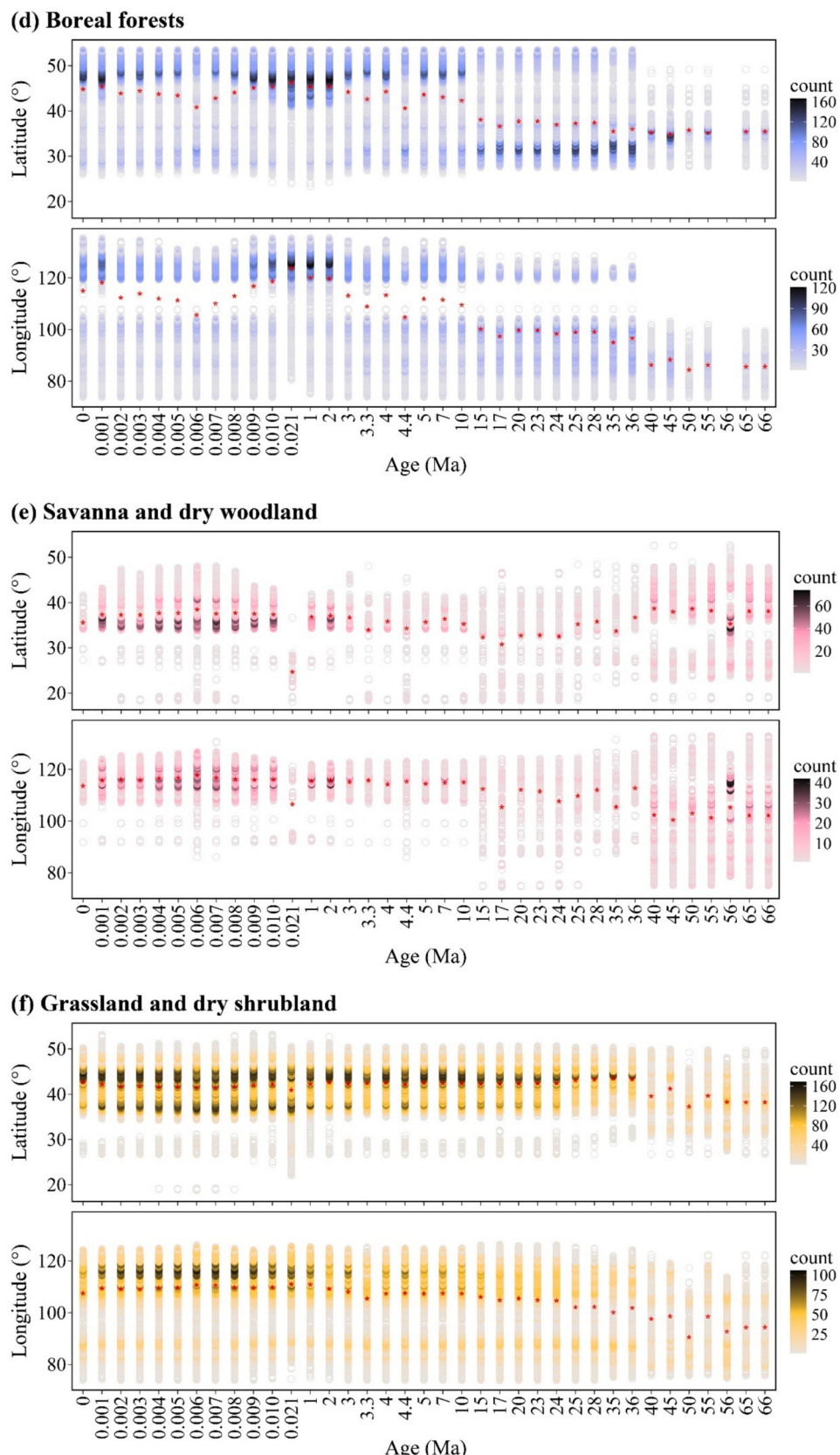
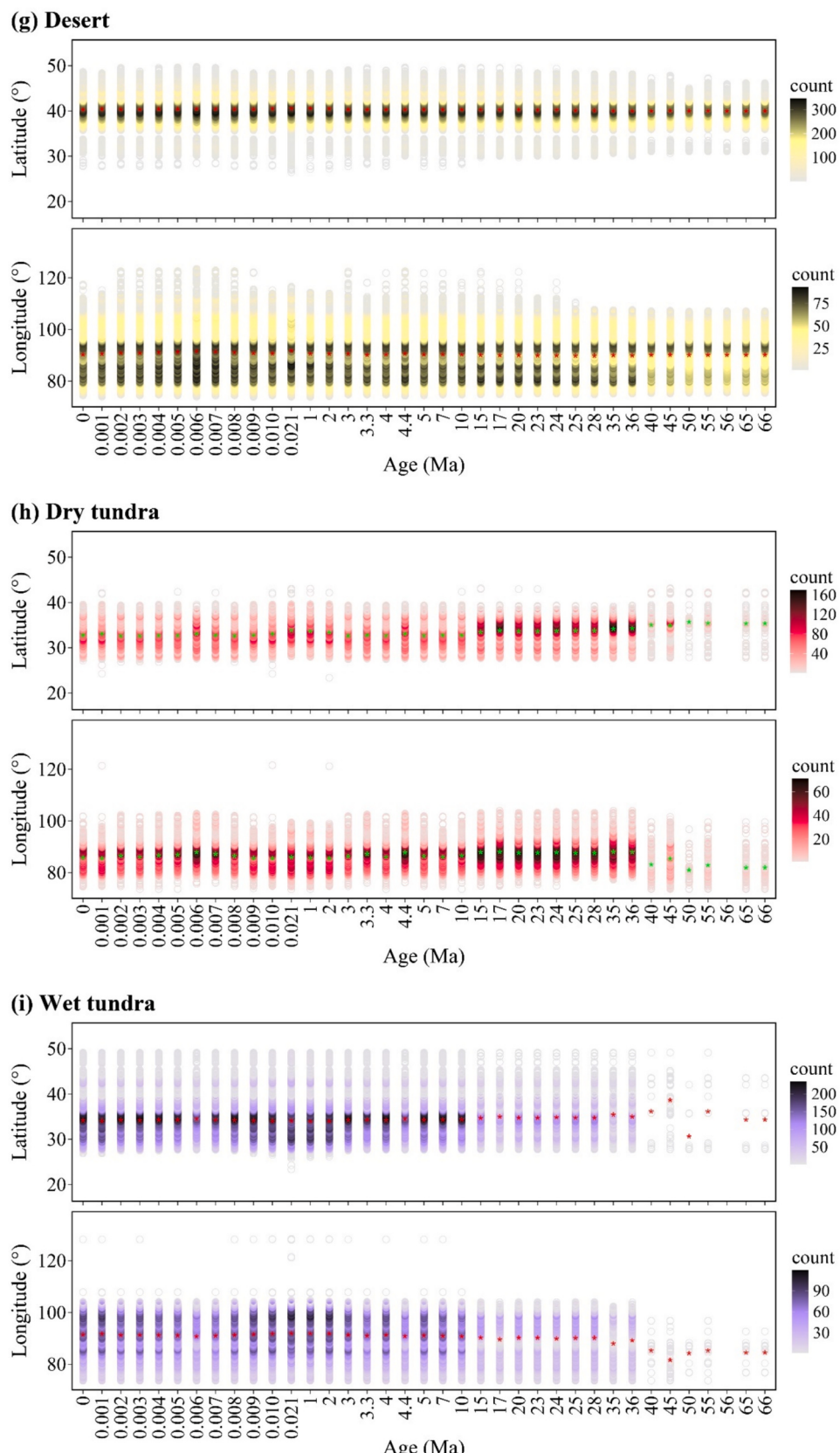


Fig. 3. (continued).

transitions on the Loess Plateau, Qaidam Basin, and Tianshan Mountains (45–34 Ma). During the 34 Ma EOT cooling, pollen showed warm shrub steppe–desert with declining shrubs and herbs and increasing conifers.

Between 34 and 15 Ma, temperate deserts and upland forests dominated, while C<sub>4</sub> vegetation expanded during the 17–15 Ma MMCO warming. From 15 Ma to 0 ka, cold-temperate herb steppe became increasingly

**Fig. 3. (continued).**

grass-dominated. Similarly, pollen-based global reconstructions at the EOT (Pound and Salzmann, 2017) indicated subtropical evergreen and warm-temperate mixed forests in northeastern China and xerophytic

shrubland in eastern China between 38 and 28 Ma. These site-level changes broadly matched our simulations, though mismatches remained.

Other paleobotanical records also support our findings. Late Paleogene (Chattian, *ca.* 25.5 Ma) lake sediments from the Lunpola Basin contained palms, indicating low elevation in central TP (Su et al., 2019). Fossil and pollen evidence from Dingqing Lake suggested montane conifers and temperate broadleaved forests mixed with subtropical evergreen species. Our simulations similarly showed encroachment of tropical, subtropical, temperate, and boreal forests, especially temperate and boreal types, into the TP interior at 25 Ma (Fig. 3).

In Yunnan Province, a 737.72-m pollen core from the Heqing Basin recorded six major vegetation-climate shifts since 2.78 Ma (Xiao et al., 2007), with rapid increases in plant diversity at 2.7–2.6 Ma and 1.18–0.34 Ma (Xiao et al., 2008). These findings align with the complex dynamics of temperate, warm-temperate, and tropical forests simulated at *ca.* 3 Ma (Fig. 3o). Likewise, a 573.39-m sediment core from the Zoige Basin on the eastern TP documented three vegetation-climate intervals over the past 1.74 Ma (Zhao et al., 2020). Between 1.74 and 1.54 Ma, conifer-deciduous forests dominated interglacials, while steppe dominated glacials. Between 1.54 and 0.62 Ma, interglacials supported conifer forest, and glacials supported meadow with increasing steppe at *ca.* 1.03 Ma. Our model predicted wet tundra at the coring site at both 1 Ma and 2 Ma, but adjacent regions contained varying mixtures of temperate grassland and forest that shifted in relative dominance between the two time slices (Fig. 3).

During the LGM, forests contracted while non-forest biomes expanded. The opposite occurred in the mid-Holocene, though range shifts were smaller (Fig. 3). These patterns were consistent with pollen-based reconstructions (Ni et al., 2014). Anthropogenic impacts on vegetation (*e.g.*, Cao et al., 2022) were not considered here.

#### 4.2. Combined effects of climate, CO<sub>2</sub> and elevation

A common biogeographical view is that vegetation distribution at regional to global scales is controlled primarily by climate factors such as heat and water. Observations, experiments, and simulations have shown that plants respond to multiple drivers, including warming, precipitation changes, elevated atmospheric CO<sub>2</sub>, nitrogen enrichment, and land use (*e.g.*, Harrison and Prentice, 2003; Parmesan and Yohe, 2003; Song et al., 2019). In this study, temperature, precipitation, and atmospheric CO<sub>2</sub> concentration jointly determined biome patterns in China throughout the Cenozoic (Fig. 2). The uplift of the TP, whether rapid or gradual, further modified regional temperature and precipitation, indirectly influencing biome shifts. During warm, humid intervals with elevated CO<sub>2</sub> (*e.g.*, 35–56 Ma; Fig. 2d–f), tropical, warm-temperate, and temperate forests expanded widely across China (Fig. 1 ac–ai), whereas boreal forests, particularly on the TP and in northeastern China (Fig. 2b), declined. Non-forest biomes such as savanna, woodland, grassland, shrubland, and tundra contracted sharply, with only minor reduction in desert extent (Fig. 2a). Forest coverage reached its maximum during this stage (Fig. 2c). In contrast, during colder, drier intervals with low CO<sub>2</sub> (*e.g.*, 9 ka to 3 Ma; Fig. 2d–f), temperate and boreal forests expanded while tropical and warm-temperate forests contracted (Fig. 1j–o). Tundra biomes increased, whereas savanna, grassland, shrubland, and desert biomes decreased substantially (Fig. 2a). Boreal forest expanded in northeastern China but contracted on the TP (Fig. 2b). Overall forest coverage reached its minimum (Fig. 2c). Under intermediate climates and CO<sub>2</sub> levels, biomes showed correspondingly moderate shifts. In general, better climatic conditions and higher CO<sub>2</sub> supported more extensive forest cover, whereas poorer conditions favored non-forest biomes. Evidence from paleovegetation records, biome modeling, and paleoclimate simulations all indicate that climate and CO<sub>2</sub> jointly regulate global vegetation distribution (Harrison and Prentice, 2003). Fossil plants (Zhao et al., 2025) and phylogenomic evidence (Qin et al., 2023) further demonstrate that vegetation in East Asia, such as evergreen broadleaved forests, exhibited heterogeneous spatiotemporal patterns under Cenozoic climate change.

Climate during the Cenozoic exhibited four states (Westerhold et al.,

2020): icehouse (0–3.3 Ma), coolhouse (3.3–34 Ma), warmhouse (34–47 Ma, 56–66 Ma), and hothouse (47–56 Ma), each accompanied by fluctuations in atmospheric CO<sub>2</sub> (Tierney et al., 2020). Past climate change, particularly abrupt shifts combined with changes in pCO<sub>2</sub>, altered ecosystem patterns. Forest biomes consistently occupied parts of China, covering 47.9 % of the land during the icehouse, 60.3 % during the coolhouse, 79.4 % during the hothouse, and 77.2 % during the warmhouse. Temperate forests were present in all four states, whereas tropical forests occurred only in the warmhouse and hothouse (Fig. 4a). Shrubland, grassland, and desert together covered a greater area in the icehouse (32.2 %) and coolhouse (26.7 %) than in the hothouse (20.4 %) or warmhouse (19.9 %). Desert consistently exceeded shrubland and grassland in extent across all states (Fig. 4a). Tundra occupied relatively small areas overall but was more extensive in the icehouse (19.9 %) and coolhouse (13.0 %) than in the hothouse (0.2 %) or warmhouse (2.9 %). Despite limited fossil and pollen records, declining temperature and pCO<sub>2</sub> clearly drove regime shifts between steppe and desert in Central Asia (Barbolini et al., 2020), a pattern also evident across much of Asia (Pound and Salzmann, 2017). Climate-driven vegetation changes, extensively documented worldwide, need not be detailed here. Past CO<sub>2</sub> concentrations were important regulators of global vegetation distribution (Harrison and Prentice, 2003) and montane forest dynamics (Jolly and Haxeltine, 1997). Higher CO<sub>2</sub> concentrations corresponded to higher temperatures (Table 1), and biome shifts in China associated with CO<sub>2</sub> changes closely paralleled those linked to climate variability (Fig. 4a).

Tectonic processes, notably the uneven uplift of the TP (Su et al., 2019), combined with the ecological advantages of C<sub>3</sub> versus C<sub>4</sub> plants (Barbolini et al., 2020), further shaped biome composition. With uplift progressing from the Paleocene to the early Pleistocene (Table 1), the TP transitioned from forest-dominated biomes (66–45 Ma, low uplift), to wet and dry tundra (45–15 Ma, medium uplift), and finally to *ca.* 75 % wet tundra and *ca.* 25 % dry tundra (15–3 Ma, high uplift). Since then, TP biomes have largely resembled modern patterns, with the positions of dry tundra in the west and forests on the eastern margin shifting with climate variability (Fig. 1). Low uplift corresponded to hothouse and warmhouse states, medium uplift to warmhouse and coolhouse states, and high uplift to coolhouse and icehouse states. These elevational changes reduced tropical and temperate forests, increased warm-temperate and boreal forests, and promoted shrubland, grassland, desert, and tundra expansion (Fig. 4b). These findings align with pollen evidence (*e.g.*, Xiao et al., 2007, 2008), macrofossil records (*e.g.*, Su et al., 2019), and phylogenomic studies (Lu et al., 2018; Ding et al., 2020; Zhou et al., 2022), all of which demonstrate the role of TP uplift in reshaping vegetation and biodiversity across China.

In summary, climate change, CO<sub>2</sub> fluctuations, and TP uplift jointly shaped vegetation dynamics in China during the Cenozoic. This conclusion is supported by our simulations, other vegetation and climate models, paleobotanical and macrofossil records, and phylogenomic evidence. These dramatic changes provide insights for assessing the risks of modern vegetation turnover under future climate scenarios and for advancing understanding of the ecological mechanisms underlying multiple environmental drivers.

#### 4.3. Uncertainties

As noted above, the input data used in this study carry limitations that introduce uncertainties into the simulations. The first source of uncertainty stems from the “artificial” paleoclimate data, which were generated by adding or subtracting fixed anomalies of temperature and precipitation to modern climate, while keeping sunshine percentage constant, rather than using transient GCM simulations. Such data cannot reflect the true magnitude, spatial distribution, or temporal variability of past climate. Although seasonal variation was included, a fixed adjustment was applied uniformly to each season.

Many studies have examined paleoclimate variability in China since

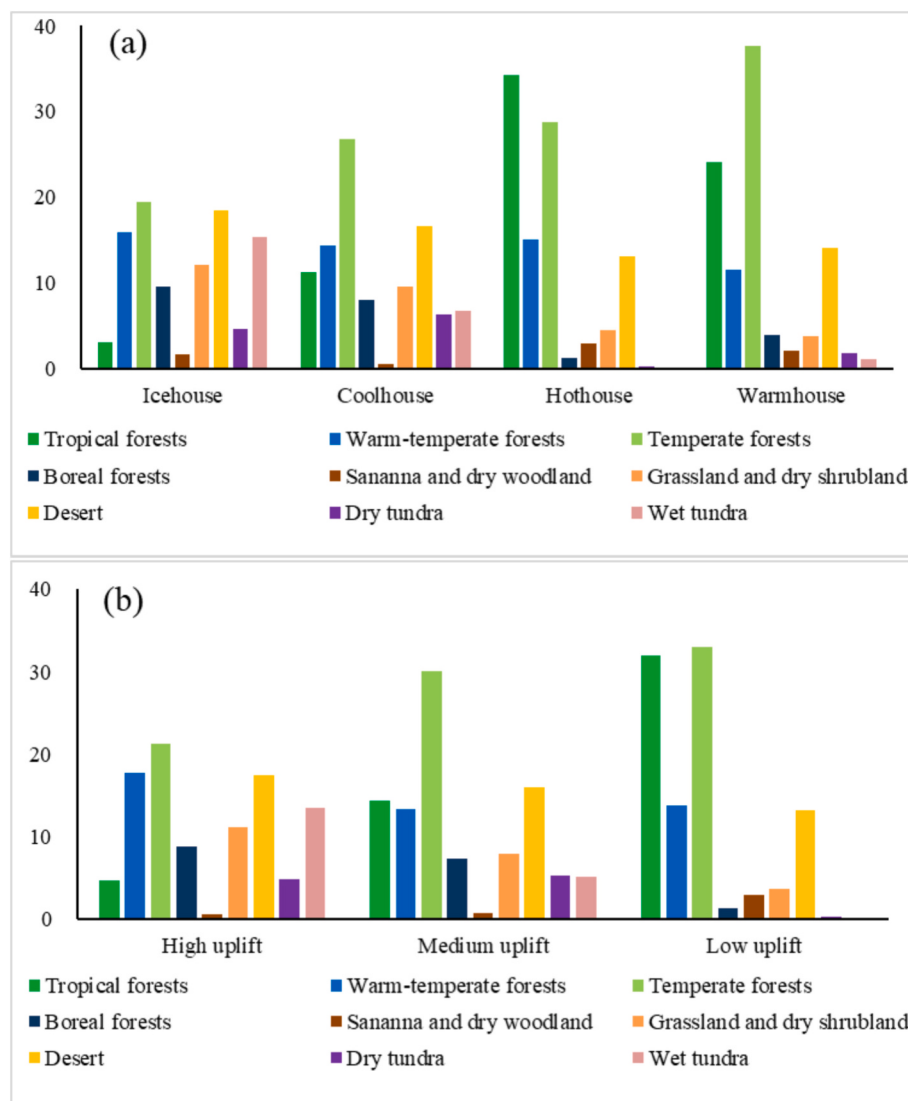


**Fig. 4.** Biome area percentages (a) across four climate states: icehouse (0–3.3 Ma), coolhouse (3.3–34 Ma), warmhouse (34–47 Ma, 56–66 Ma), and hothouse (47–56 Ma), and (b) across three TP uplift levels: high (3–15 Ma), medium (15–45 Ma), and low (45–66 Ma).

the late Pleistocene, particularly from the LGM to the Holocene, based on proxy reconstructions and climate models. While general trends are relatively well established, spatial and temporal variations remain uncertain. These include discrepancies in the magnitude and variability of climate change (e.g., Chen et al., 2020; Zhang et al., 2022; Lu et al., 2024), the timing of warming and cooling events (e.g., Liu et al., 2014; Chen et al., 2023), and mismatches between model outputs and proxy records (e.g., Jiang et al., 2012; Lin et al., 2019; Osman et al., 2021). A recent multi-proxy analysis integrating biological, geochemical, mineral, and physical evidence with regional climate simulations revealed substantial spatial variability over the past 21 ka, and highlighted both consistencies and contrasts with earlier studies (Lu et al., 2024). These discrepancies highlight the inherent uncertainties in both proxy-based reconstructions and numerical simulations (e.g., Chen et al., 2022; Karger et al., 2023).

Vegetation reconstructions and simulations also carry uncertainties. For example, vegetation often exhibits time lags in response to deglacial and mid-Holocene climate changes (Dallmeyer et al., 2022; Thompson et al., 2022). In our simulations, spatial patterns and seasonal variability were incorporated, but they were based on modern climate space, with temperature and precipitation anomalies imposed in parallel. Therefore, simulated vegetation patterns shifted uniformly with modern

vegetation, both in recent and deep times (Figs. 1, 2). Heterogeneous spatial mosaics and finer-scale changes, such as evergreen–deciduous forest replacement (Zheng et al., 2023), were not reproduced. Similarly, the expansion of grassland and desert biomes in northern China during the mid-Holocene did not match site- and region-specific pollen-based reconstructions (e.g., Ni et al., 2014). Moreover, human impacts on vegetation (e.g., Cao et al., 2022) were not considered.

For deep-time intervals, global and regional gridded proxy-based reconstructions are rare, though transient paleoclimate simulations are available for selected time slices (e.g., Farnsworth et al., 2019a, 2019b; Beyer et al., 2020; Krapp et al., 2021; Zhang et al., 2021). These simulations account for topography, land-sea distribution, ice sheets, vegetation, atmospheric CO<sub>2</sub>, solar forcing, and orbital cycles, and thus capture spatial and temporal variability more realistically. By contrast, the present study relied on fixed anomalies superimposed on modern climate, limiting the ability to represent spatial patterns in deep time. This introduced uncertainties in the simulated vegetation. Comparisons with earlier studies are constrained by the scarcity of reconstructions and simulations from 66 Ma to 3 Ma, although available comparisons show both consistencies and discrepancies in biome patterns (see Section 4.1). More broadly, simulations based on fixed anomalies produce smooth vegetation changes, whereas transient climate simulations

generate heterogeneous mosaic patterns (e.g., Allen et al., 2020; Huntley et al., 2023; Thompson et al., 2025). Even when proxy-based reconstructions are integrated with vegetation models, mismatches persist. For example, BIOME4 simulations of the Early Eocene (*ca.* 56–47.8 Ma) driven by climate model outputs showed good agreement with proxy data at low and polar latitudes but widespread discrepancies in subtropical and mid-latitude regions (Herold et al., 2014; Thompson et al., 2025). These findings highlight the persistent challenges of understanding deep-time vegetation–climate interactions.

Uncertainty also arises from precipitation anomalies. This study applied the empirical relationship of Held and Soden (2006), assuming a 7 % increase in precipitation per 1 K rise in temperature. However, a recent theoretical analysis suggested a smaller increase of *ca.* 2 % per kelvin (Cohen and Pincus, 2025). This implies that our precipitation estimates may be inflated, though broadly reasonable within the model framework.

A second major limitation concerns topography and paleogeography. TP uplift was represented as constant elevation changes across three latitudinal zones, while past land-sea boundaries were not included. This oversimplification neglects the complex tectonic and sea-level changes that characterized the Cenozoic (Scotese, 2016, 2021), and likely introduced additional uncertainties into the interpretation of biome distributions.

The paleogeographical maps of the early and middle Cenozoic, particularly from the Paleocene to the early Miocene, differed greatly from modern geography due to shifting continental latitudes, fluctuations in sea level, the opening and closure of seaways, and mountain building (Scotese, 2021). Applying a modern land-sea mask artificially enlarged land area in eastern paleo-China, especially in the southern and eastern coastal zones extending into what are now tropical to subtropical regions, while reducing land area in western paleo-China between the Himalayas and the Tarim Basin (Scotese, 2021). Therefore, simulated vegetation distributions in these regions (Fig. 1) either did not exist in reality or were spatially exaggerated, producing vegetation patterns that misrepresent Earth's history. Such a model setup introduced inaccuracies, even though the study aimed to investigate the combined effects of climate, atmospheric CO<sub>2</sub>, and topography on past vegetation change. With respect to topography, only the regional uplift of the TP was considered (Table 1), based solely on modern DEM-derived paleo-elevation. Elevational changes in other mountain systems were not included, leading to oversimplification of the complex and spatially heterogeneous uplift history of the plateau and surrounding ranges. Yet the evolution of topography and bathymetry strongly influenced global climate, ocean circulation, and the biosphere (Scotese, 2021), and also profoundly shaped regional climates and biomes in China. Using simplified paleo-elevation likely produced unrealistic biome distributions on the TP and exaggerated northward and westward biome shifts in eastern and northern China, primarily due to underestimated paleo-elevation. Moreover, vegetation predicted by the BIOME4-Asia model is highly sensitive to elevation, particularly for steppe and desert biomes in modern Central Asia (Dallmeyer et al., 2017). This likely contributed to the smaller extent of steppe–desert biome simulated across northern and western China during the Paleogene to Miocene compared with paleobotanical reconstructions (e.g., Barbolini et al., 2020; Fig. 1). These discrepancies stem from the combined limitations of paleo-elevation and climate inputs.

## 5. Conclusions

The improved and validated BIOME4-Asia global vegetation model, driven by artificially constructed past climate anomalies superimposed on modern climate space and adjusted topography, was used to simulate biome changes in China since the Cenozoic. Forest biomes expanded and shifted northward and westward at the expense of non-forest biomes during intervals of warm and humid climate, elevated pCO<sub>2</sub>, and low TP elevation, particularly from 66 Ma to 40 Ma. In contrast, during cold and

dry intervals with low pCO<sub>2</sub> and high TP elevation, especially from 2 Ma to 21 ka, forests retreated southward, grassland and desert biomes advanced eastward, and dry tundra expanded across the TP. Under milder conditions, biome changes were less pronounced, producing patterns similar to the present. In addition, abrupt regime shifts in vegetation accompanied sudden and severe environmental changes during the Cenozoic. These modeled changes broadly agree with paleovegetation simulations driven by climate model outputs and with pollen and macrofossil evidence, though discrepancies remain.

Future research should prioritize the use of “real” paleoclimate data, incorporating explicit spatial variability and transient climate dynamics from advanced climate models. Paleoogeographical constraints, including past land-sea boundaries and paleoelevation changes of the TP and other mountain systems, must be integrated to improve accuracy in reconstructing biome shifts and boundaries. Soil properties should also be considered, although such data are currently unavailable. More broadly, model inputs and boundary conditions should be derived from multiple, cross-validated sources to enhance reliability. For example, paleovegetation patterns of China over the past 20 ka have already been simulated using transient TRACE21 and CHELSA-TraCE21k climate inputs to drive BIOME4-Asia (Li et al., 2025). Extending such an approach to deep-time vegetation simulations, incorporating all relevant input variables and boundary conditions, remains a critical and challenging task for future work.

## Authors contribution

Jian Ni designed the study. Jie Xia and Jian Ni performed the simulation, interpreted the results and wrote the paper. Kai Li, Mengna Liao and Dongmei Yang interpolated the results and improved the manuscript. Zihua Tang helped the setting of BIOME4 model runs. All authors contributed to the manuscript writing.

## CRediT authorship contribution statement

**Jie Xia:** Writing – review & editing, Writing – original draft, Validation, Software, Methodology, Investigation, Formal analysis, Data curation. **Kai Li:** Writing – review & editing, Writing – original draft, Methodology, Data curation. **Mengna Liao:** Writing – review & editing, Writing – original draft, Software, Methodology, Investigation, Data curation. **Zihua Tang:** Writing – review & editing, Writing – original draft, Data curation. **Dongmei Yang:** Writing – review & editing, Writing – original draft, Validation, Investigation. **Jian Ni:** Writing – review & editing, Writing – original draft, Supervision, Methodology, Funding acquisition, Formal analysis, Data curation, Conceptualization.

## Declaration of competing interest

The authors declare that they have no known competing financial interests or personal relationships that could have appeared to influence the work reported in this paper.

## Acknowledgments

This work was supported by the Strategic Priority Research Program of the Chinese Academy of Sciences (XDB31030104), and the Ten Thousand Talents Program of Department of Science and Technology of Zhejiang Province (2018R52014). We thank an anonymous native English speaker for her/his valuable help in improving the English language of this manuscript.

## Data availability

The authors confirm that all data necessary for supporting the scientific findings of this paper have been provided.

## References

- Allen, J.R.M., Forrest, M., Hickler, T., Singarayer, J.S., Valdes, P.J., Huntley, B., 2020. Global vegetation patterns of the past 140,000 years. *J. Biogeogr.* 47, 2073–2090. <https://doi.org/10.1111/jbi.13930>.
- Barbolini, N., Wouterse, A., Dupont-Nivet, G., Silvestro, D., Tardif, D., Coster, P.M.C., Meijer, N., Chang, C., Zhang, H.X., Licht, A., Rydin, C., Koutsodendris, A., Han, F., Rohrmann, A., Liu, X.J., Zhang, Y., Donnadieu, Y., Fluteau, F., Ladant, J.-B., Le Hir, G., Hoorn, C., 2020. Cenozoic evolution of the steppe-desert biome in Central Asia. *Sci. Adv.* 6, eabb8227. <https://doi.org/10.1126/sciadv.eabb8227>.
- Beyer, R.M., Krapp, M., Manica, A., 2020. High-resolution terrestrial climate, bioclimate and vegetation for the last 120,000 years. *Sci. Data* 7, 236. <https://doi.org/10.1038/s41597-020-0552-1>.
- Cao, X.Y., Tian, F., Herzschuh, U., Ni, J., Xu, Q.H., Li, W.J., Zhang, Y.R., Luo, M.Y., Chen, F.H., 2022. Human activities have reduced plant diversity in eastern China over the last two millennia. *Glob. Chang. Biol.* 28, 4962–4976. <https://doi.org/10.1111/gcb.16274>.
- Chen, F.H., Zhang, J.F., Liu, J.B., Cao, X.Y., Hou, J.Z., Zhu, L.P., Xu, X.K., Liu, X.J., Wang, M.D., Wu, D., Huang, L.X., Zeng, T., Zhang, S., Huang, W., Zhang, X., Yang, K., 2020. Climate change, vegetation history, and landscape responses on the Tibetan Plateau during the Holocene: a comprehensive review. *Quat. Sci. Rev.* 243, 106444. <https://doi.org/10.1016/j.quascirev.2020.106444>.
- Chen, W.Z., Xiao, A.G., Braconnot, P., Ciais, P., Viovy, N., Zhang, R., 2022. Mid-Holocene high-resolution temperature and precipitation gridded reconstructions over China: Implications for elevation-dependent temperature changes. *Earth Planet. Sci. Lett.* 593, 117656. <https://doi.org/10.1016/j.epsl.2022.117656>.
- Chen, F.H., Duan, Y.W., Hao, S., Chen, J., Feng, X.P., Hou, J.Z., Cao, X.Y., Zhang, X., Zhou, T.J., 2023. Holocene thermal maximum mode versus the continuous warming mode: Problems of data-model comparisons and future research prospects. *Sci. China Earth Sci.* 66, 1683–1701. <https://doi.org/10.1007/s11430-022-1113-x>.
- Cohen, S., Pincus, R., 2025. A spectroscopic theory for how mean rainfall changes with surface temperature. *Sci. Adv.* 11, eadv6191. <https://doi.org/10.1126/sciadv.adv6191>.
- Dallmeyer, A., Claussen, M., Ni, J., Cao, X.Y., Wang, Y.B., Fischer, N., Pfeiffer, M., Jin, L., Khon, V., Wagner, S., Haberkorn, K., Herzschuh, U., 2017. Biome changes in Asia since the mid-Holocene – an analysis of different transient Earth system model simulations. *Clim. Past* 13, 107–134. <https://doi.org/10.5194/cp-13-107-2017>.
- Dallmeyer, A., Kleinen, T., Claussen, M., Weitzel, N., Cao, X.Y., Herzschuh, U., 2022. The deglacial forest conundrum. *Nat. Commun.* 13, 6035. <https://doi.org/10.1038/s41467-022-33646-6>.
- Ding, W.N., Ree, R.H., Spicer, R.A., Xing, Y.W., 2020. Ancient orogenic and monsoon-driven assembly of the world's richest temperate alpine flora. *Science* 369, 578–581. <https://doi.org/10.1126/science.abb4484>.
- Fan, J.X., Shen, S.Z., Erwin, D.H., Sadler, P.M., MacLeod, N., Cheng, Q.M., Hou, X.D., Yang, J., Wang, X.D., Wang, Y., Zhang, H., Chen, X., Li, G.X., Zhang, Y.C., Shi, Y.K., Yuan, D.X., Chen, Q., Zhang, L.N., Li, C., Zhao, Y.Y., 2020. A high-resolution summary of Cambrian to early Triassic marine invertebrate biodiversity. *Science* 367, 272–277. <https://doi.org/10.1126/science.aax4953>.
- Farnsworth, A., Lunt, D.J., Robinson, S.A., Valdes, P.J., Roberts, W.H.G., Clift, P.D., Markwick, P., Su, T., Wrobel, N., Bragg, F., Kelland, S.J., Pancost, R.D., 2019a. Past East Asian monsoon evolution controlled by paleogeography, not CO<sub>2</sub>. *Sci. Adv.* 5, eaax1697. <https://doi.org/10.1126/sciadv.aax1697>.
- Farnsworth, A., Lunt, D.J., O'Brien, C.L., Foster, G.L., Inglis, G.N., Markwick, P., Pancost, R.D., Robinson, S.A., 2019b. Climate sensitivity on geological timescales controlled by nonlinear feedbacks and ocean circulation. *Geophys. Res. Lett.* 46, 9880–9889. <https://doi.org/10.1029/2019GL083574>.
- Farr, T.G., Rosen, P.A., Caro, E., Crippen, R., Duren, R., Hensley, S., Kobrick, M., Paller, M., Rodriguez, E., Roth, L., Seal, D., Shaffer, S., Shimada, J., Umland, J., Werner, M., Oskin, M., Burbank, D., Alsford, D., 2007. The shuttle radar topography mission. *Rev. Geophys.* 45, RG2004. <https://doi.org/10.1029/2005RG000183>.
- Fordham, D.A., Jackson, S.T., Brown, S.C., Huntley, B., Brook, B.W., Dahl-Jensen, D., Gilbert, M.T.P., Otto-Biesner, B.L., Svensson, A., Theodoridis, S., Wilmsurst, J.M., Buettel, J.C., Canteri, E., McDowell, M., Orlando, L., Piliswky, J.A., Rahbek, C., Nogues-Bravo, D., 2020. Using paleo-archives to safeguard biodiversity under climate change. *Science* 369, eabc5654. <https://doi.org/10.1126/science.abc5654>.
- Foster, G.L., Royer, D.L., Lunt, D.J., 2017. Future climate forcing potentially without precedent in the last 420 million years. *Nat. Commun.* 8, 14845. <https://doi.org/10.1038/ncomms14845>.
- Gao, Q.Z., Guo, Y.Q., Xu, H.M., Ganjurjav, H., Li, Y., Wan, Y.F., Qin, X.B., Ma, X., Liu, S., 2016. Climate change and its impacts on vegetation distribution and net primary productivity of the alpine ecosystem in the Qinghai-Tibetan Plateau. *Sci. Total Environ.* 554–555, 34–41. <https://doi.org/10.1016/j.scitotenv.2016.02.131>.
- Hancock, P.A., Hutchinson, M.F., 2006. Spatial interpolation of large climate data sets using bivariate thin plate smoothing splines. *Environ. Model Softw.* 21, 1684–1694. <https://doi.org/10.1016/j.envsoft.2005.08.005>.
- Harrison, S.P., Prentice, I.C., 2003. Climate and CO<sub>2</sub> controls on global vegetation distribution at the last glacial maximum: analysis based on palaeovegetation data, biome modelling and palaeoclimate simulations. *Glob. Chang. Biol.* 9, 983–1004. <https://doi.org/10.1046/j.1365-2486.2003.00640.x>.
- Haxeltine, A., Prentice, I.C., 1996. BIOME3: an equilibrium terrestrial biosphere model based on ecophysiological constraints, resource availability, and competition among plant functional types. *Glob. Biogeochem. Cycles* 10, 693–709. <https://doi.org/10.1029/96GB02344>.
- Haxeltine, A., Prentice, I.C., Creswell, I.D., 1996. A coupled carbon and water flux model to predict vegetation structure. *J. Veg. Sci.* 7, 651–666. <https://doi.org/10.2307/3236377>.
- Held, I.M., Soden, B.J., 2006. Robust responses of the hydrological cycle to global warming. *J. Clim.* 19, 5686–5699. <https://doi.org/10.1175/JCLI3990.1>.
- Herold, N., Buzan, J., Seton, M., Goldner, A., Green, J.A.M., Müller, R.D., Markwick, P., Huber, M., 2014. A suite of early Eocene (~ 55 Ma) climate model boundary conditions. *Geosci. Model Dev.* 7, 2077–2090. <https://doi.org/10.5194/gmd-7-2077-2014>.
- Huntley, B., Allen, J.R.M., Forrest, M., Hickler, T., Ohlemüller, R., Singarayer, J.S., Valdes, P.J., 2023. Global biome patterns of the Middle and late Pleistocene. *J. Biogeogr.* 50, 1352–1372. <https://doi.org/10.1111/jbi.14619>.
- Hutchinson, M.F., Xu, T.B., 2013. ANUSPLIN Version 4.4 User Guide. Fenner School of Environment and Society, the Australian National University, Canberra, p. 52.
- IPCC, 2021. Climate Change 2021: The Physical Science Basis. Contribution of Working Group I to the Sixth Assessment Report of the Intergovernmental Panel on Climate Change. Cambridge University Press, Cambridge. <https://doi.org/10.1017/9781009157896>.
- Jiang, D.B., Lang, X.M., Tian, Z.P., Wang, T., 2012. Considerable model-data mismatch in temperature over China during the mid-Holocene: results of PMIP simulations. *J. Clim.* 25, 4135–4153. <https://doi.org/10.1175/JCLI-D-11-00231.1>.
- Jolly, D., Haxeltine, A., 1997. Effect of low glacial atmospheric CO<sub>2</sub> on tropical African montane vegetation. *Science* 276, 786–788. <https://doi.org/10.1126/science.276.5313.78>.
- Kaplan, J.O., 2001. Geophysical Applications of Vegetation Modelling. Ph.D. Dissertation. Lund University, Lund.
- Kaplan, J.O., Bigelow, N.H., Prentice, I.C., Harrison, S.P., Bartlein, P.J., Christensen, T.R., Cramer, W., Matveyeva, N.V., McGuire, A.D., Murray, D.F., Razzhivin, V.Y., Smith, B., Walker, D.A., Anderson, P.M., Andreev, A.A., Brubaker, L.B., Edwards, M.E., Lozhkin, A.V., 2003. Climate change and Arctic ecosystems: 2. Modeling, paleodata-model comparisons, and future projections. *J. Geophys. Res.-Atmos.* 108, 8171. <https://doi.org/10.1029/2002JD002559>.
- Karger, D.N., Nobis, M.P., Normand, S., Graham, C.H., Zimmermann, N.E., 2023. CHELSA-TraCE21k – high-resolution (1 km) downscaled transient temperature and precipitation data since the last Glacial Maximum. *Clim. Past* 19, 439–456. <https://doi.org/10.5194/cp-19-439-2023>.
- Krapp, M., Beyer, R.M., Edmundson, S.L., Valdes, P.J., Manica, A., 2021. A statistics-based reconstruction of high-resolution global terrestrial climate for the last 800,000 years. *Sci. Data* 8, 228. <https://doi.org/10.1038/s41597-021-01009-3>.
- Li, J.J., Fang, X.M., 1999. Uplift of the Tibetan Plateau and environmental changes. *Chin. Sci. Bull.* 44, 2117–2124. <https://doi.org/10.1007/BF03182692>.
- Li, Q., Wu, H.B., Yu, Y.Y., Sun, A.Z., Luo, Y.L., 2019. Large-scale vegetation history in China and its response to climate change since the last Glacial Maximum. *Quat. Int.* 500, 108–119. <https://doi.org/10.1016/j.quaint.2018.11.016>.
- Li, C.Z., Liu, L.N., Wang, Z.Y., Liao, M.N., Zhang, X., Li, K., Ni, J., 2025. Climate and topography jointly drove potential vegetation patterns during past 20 ka in China. *Palaeogeogr. Palaeoclimatol. Palaeoecol.*
- Lin, Y.T., Ramstein, G., Wu, H.B., Rani, R., Braconnot, P., Kageyama, M., Li, Q., Luo, Y.L., Zhang, R., Guo, Z.T., 2019. Mid-Holocene climate change over China: model–data discrepancy. *Clim. Past* 15, 1223–1249. <https://doi.org/10.5194/cp-15-1223-2019>.
- Liu, Z.Y., Zhu, J., Rosenthal, Y., Zhang, X., Otto-Biesner, B.L., Timmermann, A., Smith, R.S., Lohmann, G., Zheng, W.P., Timm, O.E., 2014. The Holocene temperature conundrum. *Proc. Natl. Acad. Sci. USA* 111, E3501–E3505. <https://doi.org/10.1073/pnas.1407229111>.
- Lu, L.M., Mao, L.F., Yang, T., Ye, J.F., Liu, B., Li, H.L., Sun, M., Miller, J.T., Mathews, S., Hu, H.H., Niu, Y.T., Peng, D.X., Chen, Y.H., Smith, S.A., Chen, M., Xiang, K.L., Le, T.-L., Dang, V.-C., Lu, A.M., Soltis, P.S., Soltis, D.E., Li, J.H., Chen, Z.D., 2018. Evolutionary history of the angiosperm flora of China. *Nature* 554, 234–238. <https://doi.org/10.1038/nature25485>.
- Lu, H.Y., Zhao, Y., Yang, X.D., Wu, H.B., Zhao, C., Wang, J.J., Wang, X.Y., Kuang, X.Y., Zhang, X.J., Ma, C.M., Lu, F.Z., Xiao, X.Y., Zhang, W.C., Wang, H.L., Xu, Z.W., Cheng, J., Zheng, Z., Shi, F., Zhang, E.L., Liang, C., Huang, Z.H., Liang, C.H., Yi, S.W., Wu, J., Shao, K.H., Gu, Y., Zhang, H.Y., Li, X.S., Han, Z.Y., Wang, X.Y., Wang, S.M., Guo, Z.T., 2024. A preliminary integrated analysis of regional paleoclimate variations in China over the past ~21 ka. *Glob. Planet. Chang.* 240, 104510. <https://doi.org/10.1016/j.gloplacha.2024.104510>.
- Lunt, D.J., Farnsworth, A., Loptson, C., Foster, G.L., Markwick, P., O'Brien, C.L., Pancost, R.D., Robinson, S.A., Wrobel, N., 2016. Palaeogeographic controls on climate and proxy interpretation. *Clim. Past* 12, 1181–1198. <https://doi.org/10.5194/cp-12-1181-2016>.
- Lüthi, D., Le Floch, M., Bereiter, B., Blunier, T., Barnola, J.-M., Siegenthaler, U., Raynaud, D., Jouzel, J., Fischer, H., Kawamura, K., Stocker, T.F., 2008. High-resolution carbon dioxide concentration record 650,000–800,000 years before present. *Nature* 453, 379–382. <https://doi.org/10.1038/nature06949>.
- Ni, J., 2000. A simulation of biomes on the Tibetan Plateau and their responses to global climate change. *Mt. Res. Dev.* 20, 80–89. [https://doi.org/10.1659/0276-4741\(2000\)020\[0080:ASOBOT\]2.0.CO;2](https://doi.org/10.1659/0276-4741(2000)020[0080:ASOBOT]2.0.CO;2).
- Ni, J., Herzschuh, U., 2011. Simulating biome distribution on the Tibetan Plateau using a modified global vegetation model. *Arct. Antarct. Alp. Res.* 43, 429–441. <https://doi.org/10.1657/1938-4246-43.3.429>.
- Ni, J., Sykes, M.T., Prentice, I.C., Cramer, W., 2000. Modelling the vegetation of China using the process-based equilibrium terrestrial biosphere model BIOME3. *Glob. Ecol. Biogeogr.* 9, 463–479. <https://doi.org/10.1046/j.1365-2699.2000.00206.x>.
- Ni, J., Cao, X.Y., Jeltsch, F., Herzschuh, U., 2014. Biome distribution over the last 22,000 yr in China. *Palaeogeogr. Palaeoclimatol. Palaeoecol.* 409, 33–47. <https://doi.org/10.1016/j.palaeo.2014.04.023>.
- Nolan, C., Overpeck, J.T., Allen, J.R.M., Anderson, P.M., Betancourt, J.L., Binney, H.A., Brewer, S., Bush, M.B., Chase, B.M., Cheddadi, R., Djemali, M., Dodson, J., Edwards, M.E., Gosling, W.D., Haberle, S., Hotchkiss, S.C., Huntley, B., Ivory, S.J.,

- Kershaw, A.P., Kim, S.-H., Latorre, C., Leydet, M., Lézine, A.-M., Liu, K.-B., Liu, Y., Lozhkin, A.V., McGlone, M.S., Marchant, R.A., Momohara, A., Moreno, P.I., Müller, S., Otto-Btiesner, B.L., Shen, C., Stevenson, J., Takahara, H., Tarasov, P.E., Tipton, J., Vincens, A., Weng, C.Y., Xu, Q.H., Zheng, Z., Jackson, S.T., 2018. Past and future global transformation of terrestrial ecosystems under climate change. *Science* 361, 920–923. <https://doi.org/10.1126/science.aan5360>.
- Osmann, M.B., Tierney, J.E., Zhu, J., Tardif, R., Hakim, G.J., King, J., Poulsen, C.J., 2021. Globally resolved surface temperatures since the last Glacial Maximum. *Nature* 599, 239–244. <https://doi.org/10.1038/s41586-021-03984-4>.
- Parmesan, C., Yohe, G., 2003. A globally coherent fingerprint of climate change impacts across natural systems. *Nature* 421, 37–42. <https://doi.org/10.1038/nature01286>.
- Pound, M.J., Salzmann, U., 2017. Heterogeneity in global vegetation and terrestrial climate change during the late Eocene to early Oligocene transition. *Sci. Rep.* 7, 43386. <https://doi.org/10.1038/srep43386>.
- Prentice, I.C., Webb III, T., 1998. BIOME 6000: reconstructing global mid-Holocene vegetation patterns from palaeoecological records. *J. Biogeogr.* 25, 997–1005. <https://doi.org/10.1046/j.1365-2699.1998.00235.x>.
- Prentice, I.C., Cramer, W., Harrison, S.P., Leemans, R., Monserud, R.A., Solomon, A.M., 1992. A global biome model based on plant physiology and dominance, soil properties and climate. *J. Biogeogr.* 19, 117–134. <https://doi.org/10.2307/2845499>.
- Prentice, I.C., Guiot, J., Huntley, B., Jolly, D., Cheddadi, R., 1996. Reconstructing biomes from palaeoecological data: a general method and its application to European pollen data at 0 and 6 ka. *Clim. Dyn.* 12, 185–194. <https://doi.org/10.1007/BF00211617>.
- Prentice, I.C., Jolly, D., Biome 6000 Participants, 2000. Mid-Holocene and glacial-maximum vegetation geography of the northern continents and Africa. *J. Biogeogr.* 27, 507–519. <https://doi.org/10.1046/j.1365-2699.2000.00425.x>.
- Prothero, D.R., 2021. Cenozoic. In: Alderton, D., Elias, S.A. (Eds.), *Encyclopedia of Geology*, Second edition. Academic Press, New York, pp. 55–61. <https://doi.org/10.1016/B978-0-12-409548-9.11847-0>.
- Qin, S.Y., Zuo, Z.Y., Guo, C., Du, X.Y., Liu, S.Y., Yu, X.Q., Xiang, X.G., Rong, J., Liu, B., Liu, Z.F., Ma, P.F., Li, D.Z., 2023. Phylogenomic insights into the origin and evolutionary history of evergreen broadleaved forests in East Asia under Cenozoic climate change. *Mol. Ecol.* 32, 2850–2868. <https://doi.org/10.1111/mec.16904>.
- Royden, L.H., Burchfiel, B.C., van der Hilst, R.D., 2008. The geological evolution of the Tibetan Plateau. *Science* 321, 1054–1058. <https://doi.org/10.1126/science.1155371>.
- Salzmann, U., Haywood, A.M., Lunt, D.J., Valdes, P.J., Hill, D.J., 2008. A new global biome reconstruction and data-model comparison for the Middle Pliocene. *Glob. Ecol. Biogeogr.* 17, 432–447. <https://doi.org/10.1111/j.1466-8238.2008.00381.x>.
- Scoates, C.R., 2016. PALEOMAP PaleoAtlas for GPlates and the PaleoData Plotter program. PALEOMAP Project. <https://www.earthbyte.org/paleomap-paleoatlas-for-gplates/>. 10.13140/RG2.2.34367.00166.
- Scoates, C.R., 2021. An atlas of Phanerozoic Paleogeographic maps: the seas come in and the seas go out. *Annu. Rev. Earth Planet. Sci.* 49, 679–728. <https://doi.org/10.1146/annurev-earth-081320-064052>.
- Shi, Y.F., Kong, Z.C., 1992. *Climates and Environments of the Holocene Mega-Thermal in China*. China Ocean Press, Beijing.
- Shi, X.Z., Yu, D.S., Warner, E.D., Pan, X.Z., Petersen, G.W., Gong, Z.G., Weindorf, D.C., 2004. Soil Database of 1:1,000,000 Digital Soil Survey and Reference System of the Chinese Genetic Soil Classification System. *Soil Surv. Horiz.* 45, 129–136. <https://doi.org/10.2136/sh2004.4.0129>.
- Sitch, S., Smith, B., Prentice, I.C., Arneth, A., Bondeau, A., Cramer, W., Kaplan, J.O., Levis, S., Lucht, W., Sykes, M.T., Thonicke, K., Venevsky, S., 2003. Evaluation of ecosystem dynamics, plant geography and terrestrial carbon cycling in the LPJ dynamic global vegetation model. *Glob. Chang. Biol.* 9, 161–185. <https://doi.org/10.1046/j.1365-2486.2003.00569.x>.
- Song, J., Wan, S., Piao, S., Knapp, A.K., Classen, A.T., Vicca, S., Ciais, P., Hovenden, M.J., Leuzinger, S., Beier, C., Kardol, P., Xia, J., Liu, Q., Ru, J., Zhou, Z., et al., 2019. A meta-analysis of 1,119 manipulative experiments on terrestrial carbon cycling responses to global change. *Nat. Ecol. Evol.* 3, 1309–1320. <https://doi.org/10.1038/s41559-019-0958-3>.
- Spicer, R.A., Farnsworth, A., Su, T., 2020. Cenozoic topography, monsoons and biodiversity conservation within the Tibetan Region: an evolving story. *Plant Divers.* 42, 229–254. <https://doi.org/10.1016/j.pld.2020.06.011>.
- Stiller, J., Feng, S.H., Chowdhury, A.-A., Rivas-González, I., Duchêne, D.A., Fang, Q., Deng, Y., Kozlov, A., Stamatakis, A., Claramunt, S., Nguyen, J.M.T., Ho, S.Y.W., Faircloth, B.C., Haag, J., Houde, P., Cracraft, J., Balabani, M., Mai, U., Chen, G., Gao, R., Zhou, C., Xie, Y., Huang, Z., Cao, Z., Yan, Z., Ogilvie, H.A., Nakhleh, L., Lindow, B., More, B., Fjeldså, J., Hosner, P.A., da Fonseca, R.R., Petersen, B., Tobias, J.A., Székely, T., Kennedy, J.D., Reeve, A.H., Likier, A., Stervander, M., Antunes, A., Tietze, D.T., Bertelsen, M.F., Lei, F., Rahbek, C., Graves, G.R., Schierup, M.H., Warnow, T., Braun, E.L., Gilbert, M.T.P., Jarvis, E.D., Mirarab, S., Zhang, G., 2024. Complexity of avian evolution revealed by family-level genomes. *Nature* 629, 851–860. <https://doi.org/10.1038/s41586-024-07323-1>.
- Su, T., Farnsworth, A., Spicer, R.A., Huang, J., Wu, F.X., Liu, J., Li, S.F., Xing, Y.W., Huang, Y.J., Deng, W.Y.D., Tang, H., Xu, C.L., Zhao, F., Srivastava, G., Valdes, P.J., Deng, T., Zhou, Z.K., 2019. No high Tibetan Plateau until the Neogene. *Sci. Adv.* 5, eaav2189. <https://doi.org/10.1126/sciadv.aav2189>.
- Sugita, S., 2007a. Theory of quantitative reconstruction of vegetation I: pollen from large sites REVEALS regional vegetation composition. *The Holocene* 17, 229–241. <https://doi.org/10.1177/0959683607075837>.
- Sugita, S., 2007b. Theory of quantitative reconstruction of vegetation II: all you need is LOVE. *The Holocene* 17, 243–257. <https://doi.org/10.1177/0959683607075838>.
- Tappronnier, P., Xu, Z.Q., Roger, F., Meyer, B., Arnaud, N., Wittlinger, G., Yang, J.S., 2001. Oblique stepwise rise and growth of the Tibet Plateau. *Science* 294, 1671–1677. <https://doi.org/10.1126/science.105978>.
- The Climate Change Center of China Meteorological Administration, 2020. *Blue Book on Climate Change in China 2020*. Science Press, Beijing, p. 102.
- The Editorial Committee of the China's National Assessment Report on Climate Change, 2007. *China's National Assessment Report on Climate Change*. Science Press, Beijing, p. 422.
- Thompson, A.J., Zhu, J., Poulsen, C.J., Tierney, J.E., Skinner, C.B., 2022. Northern Hemisphere vegetation change drives a Holocene thermal maximum. *Sci. Adv.* 8, eabj6535. <https://doi.org/10.1126/sciadv.abj6535>.
- Thompson, N., Salzmann, U., Hutchinson, D.K., Strother, S.L., Pound, M.J., Uttescher, T., Brugger, J., Hickler, T., Hocking, E.P., Lunt, D.J., 2025. Global vegetation zonation and terrestrial climate of the warm early Eocene. *Earth Sci. Rev.* 261, 105036. <https://doi.org/10.1016/j.earscirev.2024.105036>.
- Tierney, J.E., Poulsen, C.J., Montañez, I.P., Bhattacharya, T., Feng, R., Ford, H.L., Höönisch, B., Inglis, G.N., Petersen, S.V., Sagoo, N., Tabor, C.R., Thirumalai, K., Zhu, J., Burls, N.J., Foster, G.L., Goddérus, Y., Huber, B.T., Ivany, L.C., Kirtland Turner, S., Lunt, D.J., McElwain, J.C., Mills, B.J.W., Otto-Btiesner, B.L., Ridgwell, A., Zhang, Y.G., 2020. Past climates inform our future. *Science* 370, eaay3701. <https://doi.org/10.1126/science.aay3701>.
- Wang, C.S., Zhao, X.X., Liu, Z.F., Lippert, P.C., Graham, S.A., Coe, R.S., Yi, H.S., Zhu, L.D., Liu, S., Li, Y.L., 2008. Constraints on the early uplift history of the Tibetan Plateau. *Proc. Natl. Acad. Sci. U. S. A.* 105, 4987–4992. <https://doi.org/10.1073/pnas.0703595105>.
- Wang, H., Ni, J., Prentice, I.C., 2011. Sensitivity of potential natural vegetation in China to projected changes in temperature, precipitation and atmospheric CO<sub>2</sub>. *Reg. Environ. Chang.* 11, 715–727. <https://doi.org/10.1007/s10113-011-0204-2>.
- Wang, J., Pfefferkorn, H.W., Zhang, Y., Feng, Z., 2012. Permian vegetational Pompeii from Inner Mongolia and its implications for landscape paleoecology and paleobiogeography of *Cathaysia*. *Proc. Natl. Acad. Sci. U. S. A.* 109, 4927–4932. <https://doi.org/10.1073/pnas.1115076109>.
- Wang, Y.C., Lu, H.Y., Wang, K.X., Wang, Y., Li, Y.X., Clemens, S., Lv, H.Z., Huang, Z.H., Wang, H.L., Hu, X.Z., Lu, F.Z., Zhang, H.Z., 2020. Combined high- and low-latitude forcing of East Asian monsoon precipitation variability in the Pliocene warm period. *Sci. Adv.* 6, eabc2414. <https://doi.org/10.1126/sciadv.abc2414>.
- Westerhold, T., Marwan, N., Drury, A.J., Liebrand, D., Agnini, C., Anagnostou, E., Barnet, J.S.K., Bohaty, S.M., De Vleeschouwer, D., Florindo, F., Frederichs, T., Hodell, D.A., Holbourn, A.E., Kroon, D., Lauretano, V., Littler, K., Lourens, L.J., Lyle, M., Pälike, H., Röhli, U., Tian, J., Wilkens, R.H., Wilson, P.A., Zachos, J.C., 2020. An astronomically dated record of Earth's climate and its predictability over the last 66 million years. *Science* 369, 1383–1387. <https://doi.org/10.1126/science.aba6853>.
- Xiao, X.Y., Shen, J., Wang, S.M., Xiao, H.F., Tong, G.B., 2007. Palynological evidence for vegetational and climatic changes from the HQ deep drilling core in Yunnan Province. *Sci. China Ser. D-Earth Sci.* 50, 1189–1201. <https://doi.org/10.1007/s11430-007-0058-0>.
- Xiao, X.Y., Shen, J., Wang, S.M., Xiao, H.F., Tong, G.B., 2008. Plant diversity and its relationship to palaeoenvironment revealed by pollen record since 2.78 Ma in the Heqing deep drilling core. *Chin. Sci. Bull.* 53, 3686–3698. <https://doi.org/10.1007/s11434-008-0439-6>.
- Xu, T.B., Hutchinson, M.F., 2013. New developments and applications in the ANUCLIM spatial climatic and bioclimatic modelling package. *Environ. Model Softw.* 40, 267–279. <https://doi.org/10.1016/j.envsoft.2012.10.003>.
- Zhang, Q., Bernell, E., Axelsson, J., Chen, J., Han, Z., de Nootijer, W., Lu, Z., Li, Q., Zhang, Q., Wyser, K., Yang, S., 2021. Simulating the mid-Holocene, last interglacial and mid-Pliocene climate with EC-Earth3-LR. *Geosci. Model Dev.* 14, 1147–1169. <https://doi.org/10.5194/gmd-14-1147-2021>.
- Zhang, W., Wu, H., Cheng, J., Geng, J.Y., Li, Q., Sun, Y., Yu, Y.Y., Lu, H.Y., Guo, Z.T., 2022. Holocene seasonal temperature evolution and spatial variability over the Northern Hemisphere landmass. *Nat. Commun.* 13, 5334. <https://doi.org/10.1038/s41467-022-33107-0>.
- Zhao, D.S., Wu, S.H., 2014. Responses of vegetation distribution to climate change in China. *Theor. Appl. Climatol.* 117, 15–28. <https://doi.org/10.1007/s00704-013-0971-4>.
- Zhao, Y., Tzedakis, P.C., Li, Q., Qin, F., Cui, Q.Y., Liang, C., Birks, H.J.B., Liu, Y.L., Zhang, Z.Y., Ge, J.Y., Zhao, H., Felde, V.A., Deng, C.L., Cai, M.T., Li, H., Ren, W.H., Wei, H.C., Yang, H.F., Zhang, J.W., Yu, Z.C., Guo, Z.T., 2020. Evolution of vegetation and climate variability on the Tibetan Plateau over the past 1.74 million years. *Sci. Adv.* 6, eaay6193. <https://doi.org/10.1126/sciadv.aay6193>.
- Zhao, J.G., Li, S.F., Huang, J., Ding, W.N., Wu, M.X., Su, T., Farnsworth, A., Valdes, P.J., Chen, L.L., Xing, Y.W., Zhou, Z.K., 2025. Heterogeneous occurrence of evergreen broad-leaved forests in East Asia: evidence from plant fossils. *Plant Divers.* 47, 1–12. <https://doi.org/10.1016/j.pld.2024.07.004>.
- Zheng, Z., Chen, C., Huang, K.Y., Zhang, X., Kershaw, P., Cheng, J., Li, J., Yue, Y.F., Wan, Q.C., Zhang, Y.Z., Tang, Y.J., Wang, M.Y., Xiao, X.Y., Cheddadi, R., 2023. Holocene warming and evergreen/deciduous forest replacement across eastern China. *Quat. Sci. Rev.* 307, 108057. <https://doi.org/10.1016/j.quascirev.2023.108057>.
- Zhou, Z., Liu, J., Chen, L., Spicer, R.A., Li, S., Huang, J., Zhang, S., Huang, Y., Jia, L., Hu, J., Su, T., 2022. Cenozoic plants from Tibet: an extraordinary decade of

discovery, understanding and implications. *Sci. China Earth Sci.* 66, 205–226. <https://doi.org/10.1007/s11430-022-9980-9>.

Zhu, K.Z., 1973. A preliminary study of climate change in China in the past 5000 years. *Sci. China* 3, 168–189. <https://doi.org/10.1360/za1973-3-2-168>.

Zuntini, A.R., Carruthers, T., Maurin, O., Bailey, P.C., Leempoel, K., Brewer, G.E., Epitawalage, N., Françoso, E., Gallego-Paramo, B., McGinnie, C., et al., 2024. Phylogenomics and the rise of the angiosperms. *Nature* 629, 843–850. <https://doi.org/10.1038/s41586-024-07324-0>.